THE EFFECTS OF MECHANICAL TWINNING ON THE STRESS-STRAIN BEHAVIOR OF FACE-CENTERED CUBIC COPPER-TIN ALLOYS

BY

SETUMADHAVAN KRISHNAMURTHY

A DISSERTATION PRESENTED TO THE GRADUATE COUNCIL
OF THE UNIVERSITY OF FLORIDA IN PARTIAL
FULFILLMENT OF THE REQUIREMENTS FOR THE
DEGREE OF DOCTOR OF PHILOSOPHY

UNIVERSITY OF FLORIDA

1981

To my parents

Bound by DOBBS BROS. LIBRARY BINDING CO., INC., St. Augustine, Florida

ACKNOWLEDGEMENTS

I would like to express my sincere thanks and appreciation to my advisor Dr. R. E. Reed-Hill for his continued guidance, encouragement and support in all phases of this work. Thanks are also due to the members of my committee, Dr. E. D. Verink, Jr., Dr. R. T. DeHoff, Dr. E. D. Whitney and Dr. M. A. Eisenberg, for their valuable advice and helpful comments.

I wish to thank Kuang Wu Qian for his help in high temperature tests and Linda Lohmeier for drawing some of the figures. I would also like to acknowledge Barbara Smerage for her fine typing work.

The financial support for this research by the National Science Foundation under Contract Number DMR 77-22654 is gratefully acknowledged.

I am indebted to my brother, Raju, for his constant encouragement. Finally, a special note of appreciation is due to my wife, Girija, for her patience, love and understanding.

TABLE OF CONTENTS

CHAPTER PAGE

ACKNOWLEDGEMENTS iii

LIST OF FIGURES. vi

ABSTRACT xiii

1 INTRODUCTION 1

2 PREVIOUS INVESTIGATIONS. 8

2.1 Studies on Single Crystals. 8
2.2 Models for Twin Nucleation in the Face-Centered Cubic Lattice 10
2.3 Mechanical Twinning in Polycrystalline Face-Centered Cubic Metals . . .

3 EXPERIMENTAL PROCEDURE 19

3.1 Specimen Preparation. 19
3.2 Mechanical Tests. 27
3.3 Metallography 31

4 RESULTS. 33

4.1 The Stress-Strain Behavior in Tension and Compression 33
4.2 Microstructural Features and Texture Analysis. 40
4.3 The Volume Fraction of Mechanical Twins Formed in Tension and Compression 51
4.4 The Microhardness Results 64
4.5 The Effect of Mean Grain Intercept on Twinning. 69
4.6 The Temperature Dependence of Mechanical Twinning. 80

5 DISCUSSION 85

5.1 The Stress-Strain Behavior in Tension and Compression 85

5.2 Effect of Twinning on Work-Hardening Rate. 90
5.3 The Role of Microstructural Changes . . 99
5.4 The Microhardness of Twinned and Untwinned Regions 113
5.5 The Role of Deformation Temperature . . 114
5.6 The Role of Initial Boundary Area . . . 125
5.7 The Dependence of Flow Stress on Boundary Area 141
5.8 The Dependence of Flow Stress on the Intertwin Spacing 146
5.9 Suggestions for Future Work 155

6 CONCLUSIONS. 159

REFERENCES 163

BIOGRAPHICAL SKETCH. 166

LIST OF FIGURES

FIGURE		PAGE
1	Schematic diagram illustrating the effects of conventional strengthening mechanisms on the stress-strain behavior. As strength is increased, ductility decreases since plastic instability occurs sooner. . .	4
2	Thompson's tetrahedron notation for designating the slip planes and Burgers vectors in the face-centered cubic lattice	13
3	Schematic diagrams describing Vöhringer's model: (a) stress-strain curves, (b) $d\varepsilon/d\sigma$ versus σ variation	17
4	Specimen dimensions used in this investigation	21
5	Mean grain intercept versus temperature for 0.5 h annealing of Cu-4.9 at. pct. Sn. .	24
6	Mean grain intercept versus temperature for 0.5 h annealing of Cu-3.1 at. pct. Sn. . . .	26
7	Schematic representation of barreling during compression of cylinders: (a) d_o/h_o = 1, (b) d_o/h_o = 0.33.	29
8	True stress-true strain curves for Cu-4.9 at. pct. Sn alloy deformed in tension and compression at 77, 193 and 298K. The compressive stress-strain curve (dashed line) lies below the tensile curve (solid line) at each temperature.	35
9	The method of extrapolation used to correct a 298K compressive stress-strain curve for barreling. Compressive flow stresses measured on four Cu-4.9 at. pct. Sn specimens with different d_o/h_o ratios are plotted against the d_o/h_o ratio for six values of the strain. Each curve is extrapolated to d_o/h_o = 0 to obtain the flow stress corrected for barreling	37

10 Corrected compression curve is shown along with the experimental compression curve and the tensile curve for Cu-4.9 at. pct. Sn tested at 298K. The figure indicates that barreling influenced the compressive stress-strain data for true strains above 0.10 39

11 True stress-true strain curves for Cu-30 at. pct. Zn deformed in tension and compression at 298K. The compression curve (dashed line) lies below the tensile curve (solid line) for true strains above 0.03 . . 42

12 True stress-true strain curves for Co-40 at. pct. Ni tested in tension and compression at 298K. The compression curve (dashed line) lies below the tensile curve (solid line) for true strains above 0.05 . . 44

13 Photomicrograph showing the nucleation of mechanical twins at grain boundaries in a Cu-4.9 at. pct. Sn tensile specimen (d = 110 μm) deformed at 298K to a strain of 0.03. Magnification 160 times 46

14 Photomicrograph showing the transverse section of a Cu-4.9 at. pct. Sn specimen (d = 32 μm) deformed in tension to a strain of 0.20 at 298K. The twin traces intersect each other at roughly 60 degrees indicating that the structure which twins in tension has a <111> direction nearly parallel to the stress axis. Magnification 270 times. 48

15 Photomicrograph showing the transverse section of a Cu-4.9 at. pct. Sn specimen (d = 32 μm) deformed in compression to a strain of 0.10 at 298K. The twin traces make an angle of about 90 degrees with each other indicating that the structure twinning in compression has a <100> direction nearly parallel to the stress axis. Magnification 405 times. 50

16 Orientation of 25 grains for annealed Cu-4.9 at. pct. Sn alloy with a mean grain intercept of 32 μm. Data were obtained by quantitative trace analysis on a section normal to the stress axis. 53

17 Photomicrograph showing the transverse section of a Cu-4.9 at. pct. Sn alloy tensile specimen (d = 32 μm) deformed to a strain of 0.10 at 298K. Magnification 56 times . . 55

18 Photomicrograph showing the transverse section of a Cu-4.9 at. pct. Sn compression specimen (d = 32 μm) deformed to a strain of 0.10 at 298K. Magnification 56 times . . 55

19 Photomicrograph showing the transverse section of a Cu-4.9 at. pct. Sn specimen (d = 32 μm) deformed in tension to a strain of 0.07 at 298K. Magnification 270 times . . . 57

20 Photomicrograph showing the transverse section of a Cu-4.9 at. pct. Sn specimen (d = 32 μm) deformed in tension to a strain of 0.10 at 298K. Magnification 270 times . . . 57

21 Photomicrograph showing the transverse section of a Cu-4.9 at. pct. Sn specimen (d = 32 μm) deformed in tension to a strain of 0.20 at 298K. Magnification 270 times . . . 59

22 Photomicrograph showing the transverse section of a Cu-4.9 at. pct. Sn specimen (d = 32 μm) deformed in tension to a strain of 0.40 at 298K. Magnification 270 times . . . 59

23 Photomicrograph showing the transverse section of a Cu-4.9 at. pct. Sn specimen (d = 32 μm) deformed in compression to a strain of 0.02 at 298K. Magnification 405 times. . 61

24 Photomicrograph showing the transverse section of a Cu-4.9 at. pct. Sn specimen (d = 32 μm) deformed in compression to a strain of 0.065 at 298K. Magnification 270 times . 61

25 The variation of twinned volume fraction with strain for Cu-4.9 at. pct. Sn deformed in tension at 298K. 63

26 The variation of twinned volume fraction with strain for Cu-4.9 at. pct. Sn deformed in tension and compression at 298K. The volume fraction of twins is higher in the compression specimens than in the tensile specimens. 66

27 Hardness as a function of compression strain for Cu-4.9 at. pct. Sn (d = 110 μm). Initially, the <100> component has a lower hardness than the <111> component. At higher strains, however, the <100> twinned regions are harder than the untwinned <111> structure. 68

28 True stress-true strain curves for Cu-4.9 at. pct. Sn tensile specimens with various mean grain intercepts at 298K. 71

29 True stress-true strain curves for Cu-3.1 at. pct. Sn tensile specimens with various mean grain intercepts at 298K. 73

30 True stress-true strain curves for Cu-4.9 at. pct. Sn tensile specimens with various mean grain intercepts at 77K 75

31 True stress-true strain curves for Cu-3.1 at. pct. Sn tensile specimens with various mean grain intercepts at 77K 77

32 The variation of twinned volume fraction with the mean grain intercept for Cu-4.9 at. pct. Sn tensile specimens deformed to a strain of 0.25 at 298K 79

33 True stress-true strain curves for Cu-3.1 at. pct. Sn (d = 50 μm) tested in tension at various temperatures. 82

34 The variation of uniform strain (ε_u) and twinned volume fraction with test temperature for Cu-3.1 at. pct. Sn (d = 50 μm) deformed in tension. 84

35 True stress-true strain curves for Cu-4.9 at. pct. Sn alloy (d = 32 μm) at 298K. The tension and compression curves nearly coincide if the twinning strain is subtracted from the total strain. 89

36 The variation of de/dσ and dε/dσ with σ for Cu-4.9 at. pct. Sn tensile specimens. Vöhringer's results are compared with the present data. The arrows indicate the start of twinning. 92

37 The variation of dε/dσ with σ for a Co-40 at. pct. Ni (d = 50 μm) tensile specimen tested at 298K. The arrows correspond to the microstructures shown in Figures 39 to 42. 96

38 The variation of $d\varepsilon/d\sigma$ with σ with a Cu-4.9 at. pct. Sn tensile specimen (d = 32 μm) at 298K. The arrow "a" represents the start of twinning. The arrows "b" to "e" correspond to the microstructures shown in Figures 19 to 22. 98

39 Photomicrograph showing the transverse section of a Co-40 at. pct. Ni tensile specimen (d = 50 μm) deformed at 298K to a true strain of 0.14 (corresponding to the arrow "a" in Figure 37). Magnification 160 times. 102

40 Photomicrograph showing the transverse section of a Co-40 at. pct. Ni tensile specimen (d = 50 μm) deformed at 298K to a true strain of 0.16 (corresponding to the arrow "b" in Figure 37). Magnification 160 times. 102

41 Photomicrograph showing the transverse section of a Co-40 at. pct. Ni tensile specimen (d = 50 μm) deformed at 298K to a true strain of 0.20 (corresponding to the arrow "c" in Figure 37). Magnification 160 times. 104

42 Photomicrograph showing the transverse section of a Co-40 at. pct. Ni tensile specimen (d = 50 μm) deformed at 298K to a true strain of 0.27 (corresponding to the arrow "d" in Figure 37). Magnification 160 times. 104

43 The variation of $d\varepsilon/d\sigma$ with σ for a Cu-3.1 at. pct. Sn tensile specimen (d = 30 μm) at 298K. The arrows correspond to the microstructures shown in Figures 44 to 46. . 107

44 Photomicrograph showing the transverse section of a Cu-3.1 at. pct. Sn tensile specimen (d = 30 μm) deformed at 298K to a true strain of 0.18 (corresponding to the arrow "a" in Figure 43). Magnification 270 times. 109

45 Photomicrograph showing the transverse section of a Cu-3.1 at. pct. Sn tensile specimen (d = 30 μm) deformed at 298K to a true strain of 0.23 (corresponding to the arrow "b" in Figure 43). Magnification 270 times. 109

46 Photomicrograph showing the transverse section of a Cu-3.1 at. pct. Sn tensile specimen (d = 30 μm) deformed at 298K to a true strain of 0.33 (corresponding to the arrow "c" in Figure 43). Magnification 270 times. 111

47 The variation of dε/dσ with σ for a Cu-4.9 at. pct. Sn tensile specimen (d = 110 μm) tested at 77K. The arrows correspond to the microstructures shown in Figures 48 to 50 117

48 Photomicrograph showing the transverse section of a Cu-4.9 at. pct. Sn tensile specimen (d = 110 μm) deformed at 77K to a true strain of 0.01 (corresponding to the arrow "a" in Figure 47). Magnification 270 times. 119

49 Photomicrograph showing the transverse section of a Cu-4.9 at. pct. Sn tensile specimen (d = 110 μm) deformed at 77K to a true strain of 0.03 (corresponding to the arrow "b" in Figure 47). Magnification 270 times. 121

50 Photomicrograph showing the transverse section of a Cu-4.9 at. pct. Sn tensile specimen (d = 110 μm) deformed at 77K to a true strain of 0.11 (corresponding to the arrow "c" in Figure 47). Magnification 270 times. 121

51 The dependence of uniform strain on twinned volume fraction in Cu-3.1 at. pct. Sn tensile specimens (d = 50 μm). 124

52 The variation of dε/dσ with σ for Cu-4.9 at. pct. Sn tensile specimens having various mean grain intercepts at 298K. The circles represent the start of twinning. The triangles represent twin intersections within many grains 127

53 The variation of dε/dσ with σ for Cu-3.1 at. pct. Sn tensile specimens having various mean grain intercepts at 298K. 129

54 The variation of dε/dσ with σ for Cu-4.9 at. pct. Sn tensile specimens having various mean grain intercepts at 77K 131

55 The variation of $d\varepsilon/d\sigma$ with σ for Cu-3.1 at. pct. Sn tensile specimens having various mean grain intercepts at 77K. The circles represent the start of twinning. The triangles represent twin intersections within many grains 133

56 The variation of σ_t and σ_i with S_V for Cu-4.9 at. pct. Sn tensile specimens at 298K 138

57 The variation of σ_t and σ_i with S_V for Cu-3.1 at. pct. Sn tensile specimens at 77K. 140

58 The variation of ε_c and ε_i with S_V for Cu-4.9 at. pct. Sn tensile specimens at 298K 143

59 The variation of ε_c and ε_i with S_V for Cu-3.1 at. pct. Sn tensile specimens at 77K. 145

60 The variation of σ with S_V for Cu-4.9 at. pct. Sn tensile specimens deformed to various strains at 298K. The dashed lines indicate σ_t and σ_i 148

61 The variation of σ with S_V for Cu-3.1 at. pct. Sn tensile specimens deformed to various strains at 298K. 150

62 The variation of σ with S_V for Cu-4.9 at. pct. Sn tensile specimens deformed to various strains at 77K 152

63 The variation of σ with S_V for Cu-3.1 at. pct. Sn tensile specimens deformed to various strains at 77K. The dashed lines indicate σ_t and σ_i 154

64 Photomicrograph showing the surface of a Cu-4.9 at. pct. Sn tensile specimen ($d = 32\ \mu m$) which was prestrained ($\varepsilon = 0.06$), etched to show mechanical twins and restrained ($\varepsilon = 0.015$) at 298K. Mechanical twin bands are observed within an annealing twin. Inspection of the mechanical twin bands shows slip lines crossing them. Magnification 600 times. 157

Abstract of Dissertation Presented to the Graduate
Council of the University of Florida in Partial
Fulfillment of the Requirements for the
Degree of Doctor of Philosophy

THE EFFECTS OF MECHANICAL TWINNING ON THE STRESS-STRAIN BEHAVIOR OF FACE-CENTERED CUBIC COPPER-TIN ALLOYS

Setumadhavan Krishnamurthy

December 1981

Chairman: Dr. Robert E. Reed-Hill
Major Department: Materials Science and Engineering

The effects of mechanical twinning on both tensile and compressive stress-strain behavior of Cu-4.9 at. pct. Sn were investigated at 77, 193 and 298K using polycrystalline specimens with a mixed <111>-<100> wire texture. In tension, twinning occurred mainly in the <111> structure component while in compression it occurred preferentially in the <100> component in agreement with the relevant Schmid factors for twinning. The volume fraction of twins was larger in compression specimens than in tensile specimens for deformation up to a true strain of 0.20. The stress-strain curves in tension and compression differed significantly with the compression curves lying below the tensile curves. A similar effect was observed in Cu-30 at. pct. Zn and Co-40 at. pct. Ni alloys. This difference between tension and compression curves can be rationalized in terms of the effect of twinning on the stress-strain behavior.

At 298K the start of twinning was accompanied by a decrease in the work-hardening rate, since at low strains twins tend to be parallel in any given region of the structure. At larger strains the tendency for twins to form on intersecting planes should act to increase the flow stress due to grain subdivision. Microhardness data obtained from twinned and untwinned regions of Cu-4.9 at. pct. Sn compression specimens support this hypothesis. At 77K twin nucleation in Cu-4.9 at. pct. Sn occurred on intersecting planes almost from the start of the plastic region. The twinned volume fraction increased as the test temperature was lowered. Thus, a combination of high work-hardening rate and uniform elongation was observed at low temperatures.

The influence of initial grain structure on the mechanical response was studied in copper-tin specimens with mean intercepts ranging from 3.7 to 155 μm. The twinning stress increased linearly with increasing boundary area. At small strains the flow stress increased linearly with the boundary area. The variation of the flow stress was nonlinear at higher strains. This behavior has been attributed to the role of mechanical twinning.

CHAPTER 1
INTRODUCTION

An important limiting factor in the fabrication and use of metals is that when they are deformed in tension, the amount of ductility is often seriously limited by plastic instability. The deformation tends to become concentrated into a small unstable plastic region, and this phenomenon is commonly called necking. Necking often occurs at small strains so that the usefulness of a given metallic material is greatly reduced. According to Considère's criterion, necking should begin when the work-hardening rate $d\sigma/d\varepsilon$, which decreases with increasing strain, becomes equal to the stress level σ which rises with increasing strain ε. This condition defines the magnitude of the uniform strain ε_u and, since in most cases of commercial importance the necking strain is small compared to ε_u and tends to be fixed in magnitude, the total elongation is also largely determined by Considère's criterion.

It goes without saying that a set of mechanical properties combining high strength with high ductility is desirable. Unfortunately, as pointed out by Zackay et al.,[1] "a major part of both the theoretical and experimental evidence accumulated to date suggests that strength and ductility are inversely related" (p. 252). The inherent tendency for strength to be inversely related to ductility can be qualitatively rationalized on the basis that many of our better known strengthening mechanisms do not significantly change the way $d\sigma/d\varepsilon$ changes with ε. Thus, for example, hardening steel by a quench and temper while increasing the yield stress does not appreciably alter the rate of work-hardening.[1] This effect is indicated schematically in Figure 1. This diagram shows four stress-strain curves for steels which were tempered to various strength levels. It is evident that when the strength is increased, the ductility is reduced since the condition $\sigma = d\sigma/d\varepsilon$ is satisfied sooner.

Any mechanism that would tend to decrease the rate of fall with strain of the work-hardening rate should allow the stress level and accordingly the strain before the onset of necking to increase. Full advantage of this hypothesis is taken in designing the well known TRIP (transformation induced plasticity) steels. While these steels may receive a large prior deformation in the austenite range in order to raise their strength level to the order of 1400 M Pa or higher,[2] their inherent ductility at ambient temperatures is associated with the formation of martensite platelets in the structure during deformation.

It has recently been recognized that an analogous method of reducing the rate of decrease of the work-hardening rate with strain is offered by mechanical twinning. Garde and Reed-Hill[3] reported stress-strain data showing a combination

Figure 1

Schematic diagram illustrating the effects of conventional strengthening mechanisms on the stress-strain behavior. As strength is increased, ductility decreases since plastic instability occurs sooner.

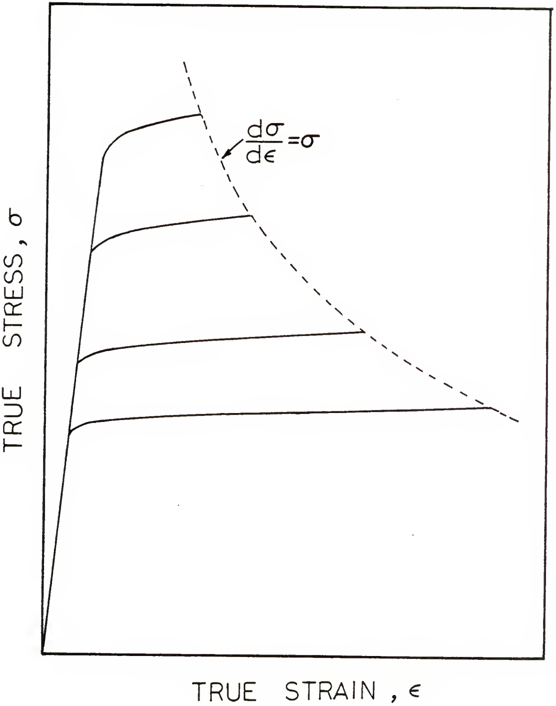

$\frac{d\sigma}{d\epsilon}=\sigma$
TRUE STRESS, σ
TRUE STRAIN, ϵ

of a high ultimate tensile strength with a large uniform elongation for high purity titanium specimens deformed at 77K. They also found extensive twinning in this case. There is evidence that twinning can also increase the uniform strain in body-centered cubic metals. This has been demonstrated by the data of Loria et al.[4] for vanadium and by Reid et al.[5] for niobium. A strong effect of twinning on the basic work-hardening rate has also been observed in a number of low stacking fault energy face-centered cubic metals and alloys. Carreker's[6] data for silver showed that the uniform strain ε_u tends to increase with decreasing test temperature. In this case, the rate of decrease of $d\sigma/d\varepsilon$ with ε is smaller the lower the temperature. As a consequence both ε_u and the ultimate tensile strength increase with decreasing temperature. The ability of twinning to increase the uniform strain and the ultimate strength has thus been observed in metals of all three basic metallic crystal structures.

In face-centered cubic metals and alloys the effect of twinning on the basic work-hardening rate has possible commercial significance. Not only is this effect strong, but it can appear in most of the commercially important alloys of this type such as the brasses, the various bronzes (silicon, aluminum and tin) and many other alloys including those of nickel and cobalt that form the basis for the matrix of high temperature high strength superalloys. It has been claimed[7-9] that the Hadfield manganese steel forms mechanical twins in the austenite or the face-centered cubic phase. The unusual work-hardening characteristics of this material are universally recognized. The high mechanical properties of this steel have been attributed to the formation of mechanical twins.

While there have been many investigations of mechanical twinning in face-centered cubic metallic systems, very little work has been devoted to determining the effect of twinning on the stress-strain behavior. Most of the previous studies dealt with single crystals of pure metals deformed at very low temperatures. Research on twinning in polycrystalline materials has been very limited. A review of the literature concerning the role of mechanical twinning revealed that several areas require a more thorough investigation. There is uncertainty as to whether the work-hardening rate is increased or decreased by twinning. The role of fiber texture in polycrystalline deformation has been completely ignored by previous workers. The influence of grain size on twinning has not been investigated in detail. These areas constitute the focus of attention in this investigation.

It is well-known that the stacking fault energy is one of the most important factors which control twinning stesses. The twinning stress decreases with increasing alloy content or with decreasing stacking fault energy. Therefore, the materials used in the present work were low stacking fault energy face-centered cubic alloys. A major part of this study was carried out by using alpha copper-tin alloys. The occurrence of mechanical twinning in these alloys has been confirmed by Baker and Peters[10] with the aid of selected area electron diffraction. Another criterion used in selecting the copper-tin alloys was that the mechanical twins produced were easily resolved in an optical microscope and thus well-suited for quantitative analysis. Some additional work was conducted on nickel-cobalt and copper-zinc alloys.

The results obtained in this investigation show several significant factors not previously recognized about the effects of mechanical twinning on the stress-strain behavior of polycrystalline face-centered cubic metals and alloys.

CHAPTER 2
PREVIOUS INVESTIGATIONS

2.1 Studies on Single Crystals

Mechanical twinning had long been considered as irrelevant to the deformation mechanisms of face-centered cubic metals. This was due to the fact that the study of deformation mechanisms had been limited to single crystals of pure face-centered cubic metals which unfortunately do not twin readily even at low temperatures because of their high stacking fault energies. In fact, in 1951, Cottrell and Bilby[11] proposed a twin nucleation model which concluded that mechanical twins cannot be produced in the face-centered cubic lattice. However, in 1957, Blewitt et al.[12] showed that twins form during the tensile testing of copper crystals at very low temperatures (4.2K) and they also found mechanical twins in silver and gold crystals. Since the early work of Blewitt et al., mechanical twinning has been observed in single crystals of nickel,[13] silver-gold alloys,[14,15] copper-gallium and copper-germanium alloys,[16,17] copper-zinc alloys,[18] copper-aluminum,[19] cobalt-iron[20] and in alloys of silver with indium, cadmium and tin.[21]

The various observations from the studies on single crystals can be summarized as follows:

1. The twinning in face-centered cubic metals occurs on {111} planes along <11$\overline{2}$> directions. The twinning shear is 0.707.
2. The smooth portion of the load-elongation curve is terminated by a load drop accompanied by an audible click when twin nucleation occurs. Blewitt et al.[12] reported this load drop in their work on copper single crystals. This has been confirmed by Suzuki and Barrett[14] in their studies using silver-gold alloy crystals, and by many other workers. In copper-zinc alloys, Thornton and Mitchell[18] found that the stress drop observed on twinning decreases with decreasing deformation temperature. The results of Narita and Takamura[21] show that in high concentration alloys such as Ag-8 at. pct. In, a load drop due to twinning is not observed on the load-elongation curve, but an inflection point appears instead.
3. The orientation dependence has been studied by many investigators. It has been shown that the twinning stress decreases as the tensile axis approaches the [111] tensile direction. Twinning is usually not observed in crystals with a [100] tensile orientation.
4. The critical twinning stress decreases with increasing amount of the alloying element or with decreasing stacking fault energy.

5. Studies on silver single crystals[15] showed that the twinning stress is a function of deformation temperature. The twinning stress increased by a factor of two when the temperature was raised from 4 to 300 K. However, no systematic temperature dependence of the twinning stress was found in copper-germanium and copper-gallium alloys studied by Haasen and King.[16]

2.2 Models for Twin Nucleation in the Face-Centered Cubic Lattice

Slip and twinning are the two fundamental modes of plastic deformation in metals and alloys. Slip occurs when crystal planes glide past each other. This is achieved by the passage of dislocations on different slip planes. Since the Burgers vector of the slip dislocations is always a lattice vector, the atoms move from one lattice site to an adjacent equivalent one during slip. Therefore, the slipped and unslipped regions have identical orientation. On the other hand, according to the definition of twinning adopted by Bilby and Crocker:[22] "a deformation twin is a region of a crystalline body which has undergone a homogeneous shape deformation in such a way that the resulting product structure is identical with that of the parent, but oriented differently" (p. 240). The formation of a twin can be accomplished by the passage of twinning partials on successive twin planes. The Burgers vector of these partials is always some fraction of the lattice vector.

The general arguments for a dislocation mechanism of mechanical twinning are the same as those for slip. First, it is scarcely believable that the atoms concerned should all move simultaneously, and second, twinning takes place at stresses far below the theoretical shear strength of a perfect lattice. The atomic movements required to produce the twinned lattice from the original one are generally more complicated than those that produce slip.

In order to discuss the models for twinning, it is convenient to use the reference tetrahedron of Thompson[23] to designate the slip planes and Burgers vectors in the face-centered cubic lattice. This is shown in Figure 2. The first dislocation mechanism for twinning in the face-centered cubic lattice was suggested by Cottrell and Bilby.[11] They considered the dissociation of a length of the dislocation AC into the Frank partial Aα and the twinning dislocation αC. The dislocation AC forms a "pole" where it leaves the plane (a), and the dislocation αC rotates around this pole, returning to meet Aα. Cottrell and Bilby proposed that the twinning dislocation could go no further as it is obstructed by the dislocation Aα. Hence, single layer faults but not twins could be produced in face-centered cubic metals. These conclusions were especially satisfying because, at that time, no one had demonstrated unambiguously that mechanical twinning could occur in these metals. This mechanism was extended by Venebles[24] to account for the production of twins. Venebles proposed that after one

Figure 2

Thompson's tetrahedron notation for designating the slip planes and Burgers vectors in the face-centered cubic lattice.

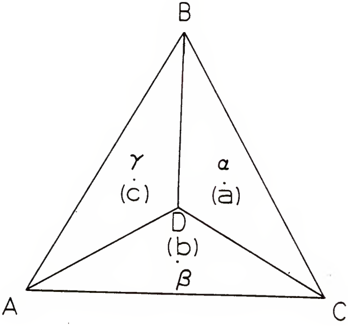
B
γ
(ċ)
α
(ȧ)
D
(ḅ)
β
A
C

revolution around the pole, the twinning dislocation meets the dislocation Aα and recombines to form AC again. This whole dislocation can move along its glide cylinder and redissociate at the next atomic plane. In this way, a twin of finite thickness can be built from a single stacking fault.

Many other models[14,25,26] have been proposed in order to explain the nucleation of twins in face-centered cubic metals. However, at present, there is no general agreement concerning the dislocation mechanism for twin nucleation in face-centered cubic metals.

2.3 Mechanical Twinning in Polycrystalline Face-Centered Cubic Metals

The nature of the role that twinning plays in the development of the stress-strain curve of low stacking fault energy polycrystalline face-centered cubic metals is far from resolved. In fact, two very divergent points of view have evolved. In one due to Vöhringer,[27-30] it is assumed that the formation of a twin adds an increment to the strain but does not influence the flow stress. Briefly, this would have the effect of lowering the work-hardening rate once twinning begins. Vöhringer has made use of plots of the reciprocal of the work-hardening rate $d\varepsilon/d\sigma$ versus the stress in which a sudden increase in $d\varepsilon/d\sigma$ is used to define the point on a stress-strain curve at which twinning commences. Vöhringer's model is shown schematically in

Figure 3. In Figure 3(a) twin nucleation occurs at the stress σ_t (or at a critical strain ε_c) and beyond this point there is a decrease in the work-hardening rate. This decrease is represented by the shaded region in Figure 3(b). Vöhringer worked on polycrystalline alpha copper alloys using optical microscopy and he has reported that the first twin lamellae became visible at the point (σ_t) corresponding to the sudden increase of $d\varepsilon/d\sigma$ in the $d\varepsilon/d\sigma$ versus σ plot. Rémy,[31] who has studied cobalt-33 wt. pct. nickel, has taken an alternative point of view. He assumes that twinning increases the flow stress due to the fact that the twin boundaries increase the total boundary area per unit volume. In other words, the flow stress is increased by twinning due to a decrease in the effective grain size. According to Rémy's hypothesis, twinning should act to increase the work-hardening rate and not decrease it as proposed Vöhringer.

A major part of the present study was devoted to differentiate between these two opposing points of view. The role of fiber texture which has been completely ignored by the previous workers was also explored in the current investigation. It was planned to test specimens having a strong <111> fiber texture. (A strong <100> texture was a suitable alternative.) The purpose of this requirement was to take advantage of the fact that both <111> and <100> are stress axis orientations where the ease of twinning should differ significantly between specimens tested in

Figure 3

Schematic diagrams describing Vöhringer's model:
(a) stress-strain curves, (b) $d\varepsilon/d\sigma$ versus σ variation.

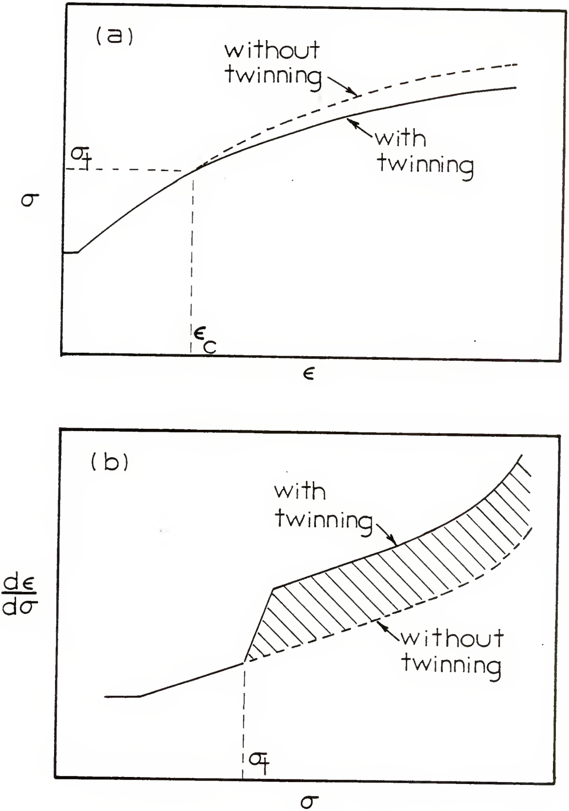
(a)
without twinning
with twinning
σ_t
σ
ε_c
ε
(b)
with twinning
without twinning
dε/dσ
σ_t
σ

tension and compression. Thus a tensile and a compression test made on the same type of specimen should give two stress-strain curves whose difference is directly relatable to a difference in the degree of twinning that occurred in the specimens.

CHAPTER 3
EXPERIMENTAL PROCEDURE

3.1 Specimen Preparation

The copper-tin alloys used in this work were prepared by the Materials Research Corporation using VP grade (99.998 pct. purity) elemental materials. A major part of the experimental work was carried out by using a Cu-4.9 at. pct. Sn alloy. Another copper-tin alloy that was used in some tests contained 3.1 at. pct. Sn. The as-received cast rods of these alloys were first given a 24 hour homogenization anneal at 993K. They were next machined from 25.4 mm to 24.4 mm diameter and then swaged through successive dies to a final diameter of 6.35 mm. An intermediate annealing at 993K for 4 hours was necessary when the diameter had been reduced to 19.05 mm. The resulting swaged rods were machined into tension and compression test specimens.

Two types of tensile specimens were used. Figure 4(a) shows a threaded-end tensile specimen with 3.8 by 20.3 mm cylindrical gage section. Specimens of this type were used in obtaining the stress-strain curves. Transverse sections of these samples were used for metallographic examination. The other type of tensile specimens had flat sides in the gage section. Such a specimen is shown in Figure 4(b).

Figure 4

Specimen dimensions used in this investigation.

All dimensions in mm

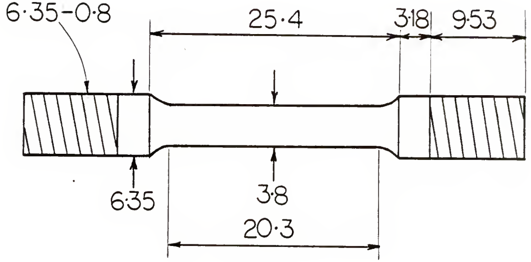

(a)

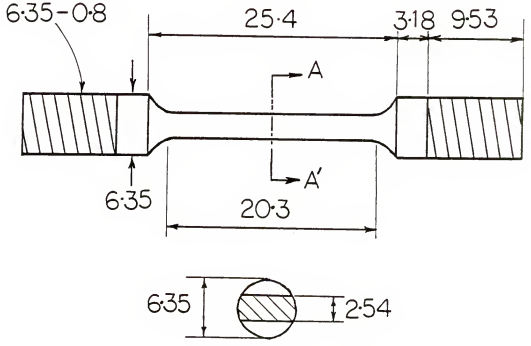

Section AA'
(b)

This type was useful when it was necessary to examine the structural features as a function of the strain within a single specimen.

The compression test specimens were cylinders with a diameter of 6.35 mm and a height of 15.9 mm. The gage lengths of four of the compression specimens were varied to obtain different d_o/h_o ratios between 0.4 and 3.2 (d_o = diameter and h_o = height of the cylinder).

The cold-worked structure was recrystallized and a range of mean grain intercepts between 3.7 μm and 125 μm was obtained by 0.5 hour anneals at the appropriate temperatures. The effect of annealing temperature on the mean grain intercept is shown in Figures 5 and 6 for the Cu-4.9 at. pct. Sn and Cu-3.1 at. pct. Sn alloys, respectively. In addition, some Cu-3.1 at. pct. Sn specimens were annealed at 1123K for 1.5 hours to obtain a mean intercept of 155 μm. Annealing twin boundaries as well as grain boundaries were counted in determining the mean intercepts.

Additional tests were conducted on Cu-30 at. pct. Zn and Co-40 at. pct. Ni alloys which were available in this laboratory. The copper-zinc alloy rods were swaged through successive dies from an initial diameter of 22 mm to a final diameter of 6.35 mm. The swaged rods were machined into tensile specimens of the types shown in Figure 4 and cylindrical compression specimens with 6.35 mm by 15.5 mm gage sections. These samples were annealed at 923K for 0.5 hour and a mean grain intercept of 30 μm was obtained.

Figure 5

Mean grain intercept versus temperature for 0.5 h annealing of Cu-4.9 at. pct. Sn.

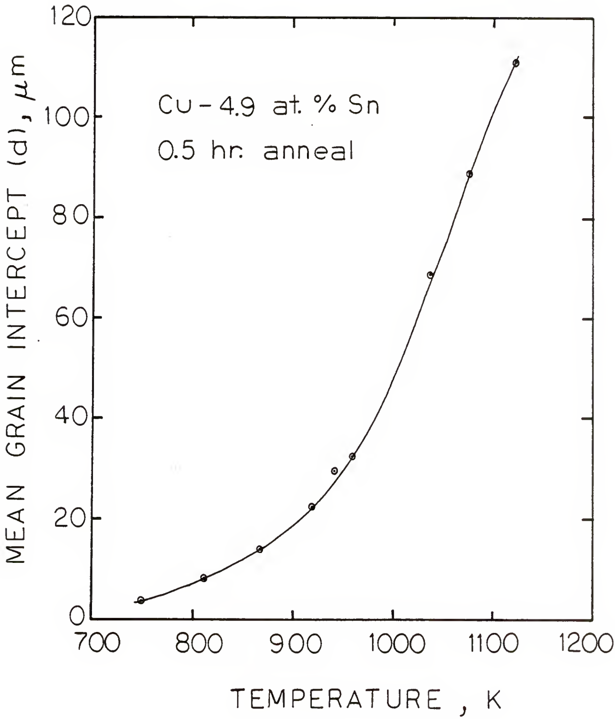
Cu - 4.9 at. % Sn
0.5 hr. anneal
MEAN GRAIN INTERCEPT (d), μm
0
20
40
60
80
100
120
700
800
900
1000
1100
1200
TEMPERATURE , K

Figure 6

Mean grain intercept versus temperature for 0.5 h annealing of Cu-3.1 at. pct. Sn.

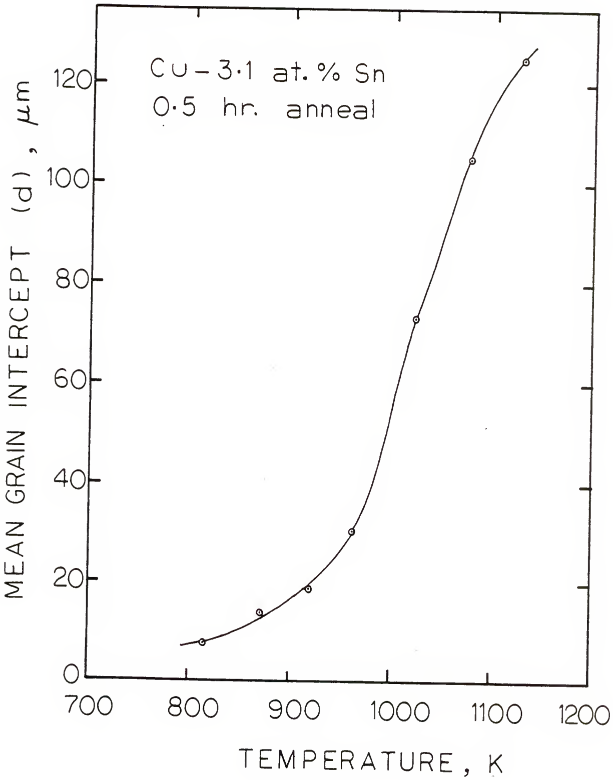
Cu – 3·1 at. % Sn
0·5 hr. anneal
MEAN GRAIN INTERCEPT (d), μm
0
20
40
60
80
100
120
700
800
900
1000
1100
1200
TEMPERATURE, K

The cobalt-nickel alloy was in the form of 5.59 mm diameter swaged rods. These rods were machined into cylindrical threaded-end tensile specimens with a gage diameter of 3.5 mm and a gage length equal to 17.3 mm. Compression specimens of this material were cylinders with 3.5 mm by 8.33 mm gage sections. These cobalt-nickel alloy specimens were vacuum-annealed at 1273K for 0.5 hour resulting in a mean grain intercept of 50 μm.

3.2 Mechanical Tests

The annealed Cu-4.9 at. pct. Sn alloy specimens with a mean grain intercept of 32 μm were deformed at 77, 193 and 298K on an Instron testing machine using a 0.508 mm per minute cross-head speed. True stress versus true strain curves and their slopes at various plastic strains were derived from load-time charts. The tensile curves were plotted only up to the maximum load. The determination of true stress-true strain curves under compression is complicated by the frictional effects between the tool-steel platens and the test specimen which give rise to a barreling effect. The material adjacent to the platens undergoes little or no deformation and this effect extends to some depth into the cylinder. The barreling effect becomes progressively less with increasing height of the cylinder. This is illustrated in Figure 7. However, it is not possible to obtain satisfactory results with cylinders having $d_o/h_o < 0.4$ because of buckling. The d_o/h_o ratios used in

Figure 7

Schematic representation of barreling during compression of cylinders: (a) $d_o/h_o = 1$, (b) $d_o/h_o = 0.33$.

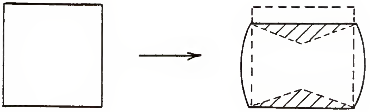

(a)

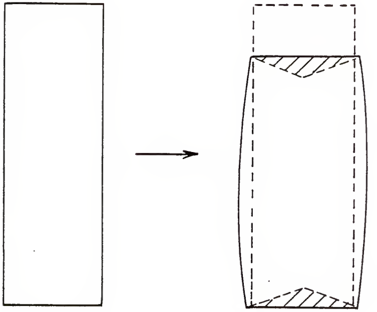

(b)

the present tests were very close to 0.4. In all compression tests Teflon tape was used as a lubricant at the surfaces of contact between the specimen and the platens. The compressive stress-strain curves were plotted only up to true strain levels of about 0.25 because above this strain barreling became significant. In order to determine quantitatively how large an effect barreling had on the stress-strain curve below a true strain of 0.25, a room temperature compression curve was corrected for barreling using the graphical extrapolation method of Cook and Larke.[32] In this method, the true flow stress or yield stress in compression is found by extrapolating the measured average stress for a number of specimens of different geometry to a diameter to height ratio of zero.

Some Cu-4.9 at. pct. Sn alloy compression samples were annealed at 1123K for 0.5 hour to obtain a mean grain intercept of 110 μm. These were used to measure the hardness of the material in grains that had twinned and those that had not twinned. These specimens were compressed to various strains, sectioned normal to the stress axis and then microhardness measurements were made on the polished transverse sections using a 136 degree diamond pyramid indentor.

Additional tension and compression data were obtained by testing the cobalt-nickel and copper-zinc specimens at 298K. The influence of initial boundary area and deformation temperature on the twinning process was also studied in the copper-tin alloys.

3.3 Metallography

Deformed copper-tin alloy specimens were electropolished in a well-stirred solution of 50 g $Cu(NO_3)_2 \cdot 3H_2O$, 5 ml HNO_3 and 150 ml CH_3OH cooled in a mixture of ice and water. They were then etched in a solution containing equal parts of water, nitric acid and 25 pct. glacial acetic acid. This etching resulted in surfaces responsive to polarized light. The use of polarized light led to a clear resolution of the mechanical twins. The advantage of using polarized light in the metallographic examination of face-centered cubic metals has been discussed in detail by Reed-Hill et al.[33]

The volume fraction of mechanical twins was measured on transverse sections of deformed specimens by point-counting using a 5 x 5 square grid within the ocular of the metallograph. The volume fraction measurements were based on the number of grid-line intersections that fell over the mechanical twins in randomly selected regions of the sections. Forty to forty-five regions were used for each measurement. The statistical errors associated with the averages were estimated by using standard techniques.[34]

The twin traces observed optically on surfaces normal to the stress axis were also used to characterize the fiber texture of the specimens. With the aid of measurements of the angles between {111} twin traces, the orientations of individual grains relative to the stress axis were determined following the method of Drazin and Otte.[35] A measurement at 10 pct. strain of the volume fraction of the grains which were twinned in the tensile and compressive specimens respectively also gave volume fractions which were in close agreement with the results of trace analysis.

The nickel-cobalt microstructures were analyzed by electropolishing the transverse sections in a solution containing 60 ml HCl, 15 ml HNO_3, 15 ml glacial acetic acid and 15 ml H_2O at room temperature. The polished samples were etched with a solution of 15 drops of 48 pct. HF in 20 ml HNO_3.

CHAPTER 4
RESULTS

4.1 The Stress-Strain Behavior in Tension and Compression

The tensile and compressive true stress-true strain curves obtained at 77, 193 and 298K for the Cu-4.9 at. pct. Sn alloy with a mean grain intercept of 32 μm are shown in Figure 8. It is evident that at each temperature the compressive stress-strain curve lies below the tensile curve. The compression data shown in this figure have to be corrected to eliminate the effect of barreling. Figure 9 shows the method of extrapolation used to correct a 298K compressive stress-strain curve for barreling. Here the flow stress, measured for four specimens of different d_o/h_o ratios, is plotted against the d_o/h_o ratio for six values of the strain ε ranging from 0.01 to 0.25. Extrapolation of each curve to $d_o/h_o = 0$, corresponding to a hypothetical specimen of infinite length, gives a value of the flow stress corrected for barreling. The resulting corrected stress-strain curve plotted in Figure 10 represents the condition of homogeneous compression. Note that in this figure, the corrected compression curve lies below the experimental compression curve. It may also be seen that barreling influenced the compression stress-strain data for

Figure 8

True stress-true strain curves for Cu-4.9 at. pct. Sn alloy deformed in tension and compression at 77, 193 and 298K. The compressive stress-strain curve (dashed line) lies below the tensile curve (solid line) at each temperature.

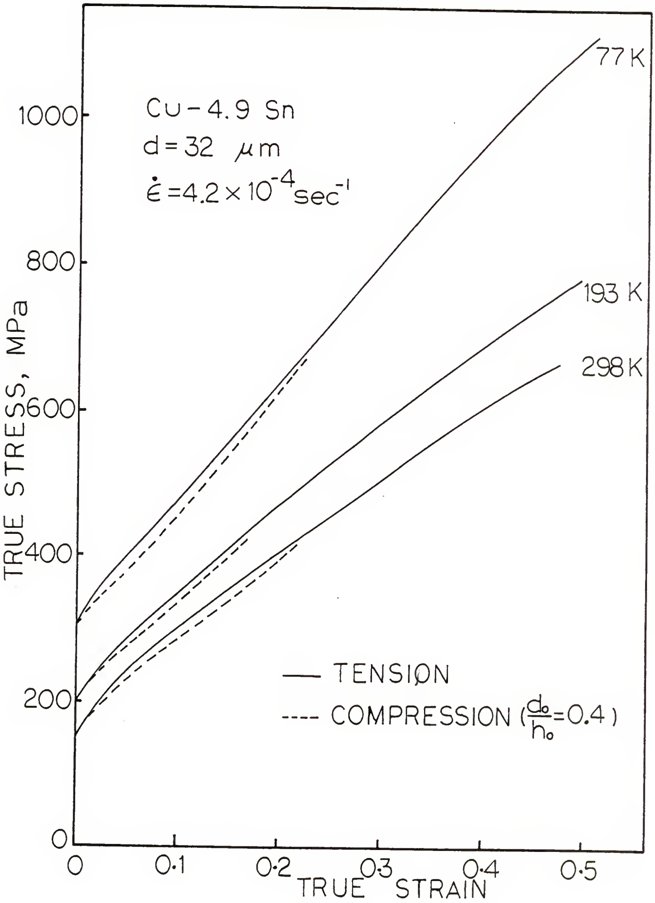
Cu-4.9 Sn
d=32 μm
ε̇=4.2×10⁻⁴sec⁻¹
77 K
193 K
298 K
TENSION
COMPRESSION (d₀/h₀=0.4)
TRUE STRESS, MPa
0
200
400
600
800
1000
TRUE STRAIN
0
0·1
0·2
0·3
0·4
0·5

Figure 9

The method of extrapolation used to correct a 298K compressive stress-strain curve for barreling. Compressive flow stresses measured on four Cu-4.9 at. pct. Sn specimens with different d_o/h_o ratios are plotted against the d_o/h_o ratio for six values of the strain. Each curve is extrapolated to $d_o/h_o = 0$ to obtain the flow stress corrected for barreling.

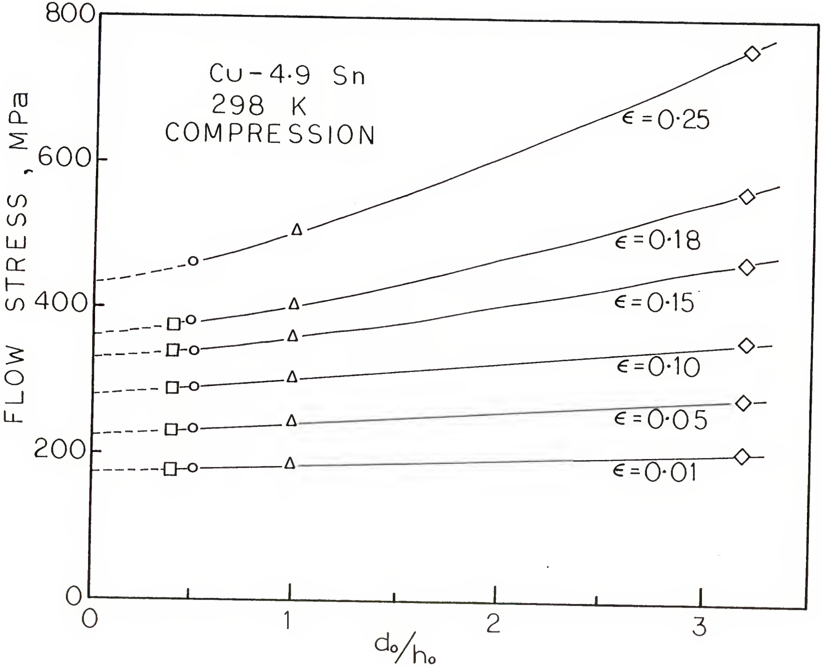
Cu-4·9 Sn
298 K
COMPRESSION
FLOW STRESS, MPa
800
600
400
200
0
0
1
2
3
d_o/h_o
$\epsilon = 0\cdot25$
$\epsilon = 0\cdot18$
$\epsilon = 0\cdot15$
$\epsilon = 0\cdot10$
$\epsilon = 0\cdot05$
$\epsilon = 0\cdot01$

Figure 10

Corrected compression curve is shown along with the experimental compression curve and the tensile curve for Cu-4.9 at. pct. Sn tested at 298K. The figure indicates that barreling influenced the compressive stress-strain data for true strains above 0.10.

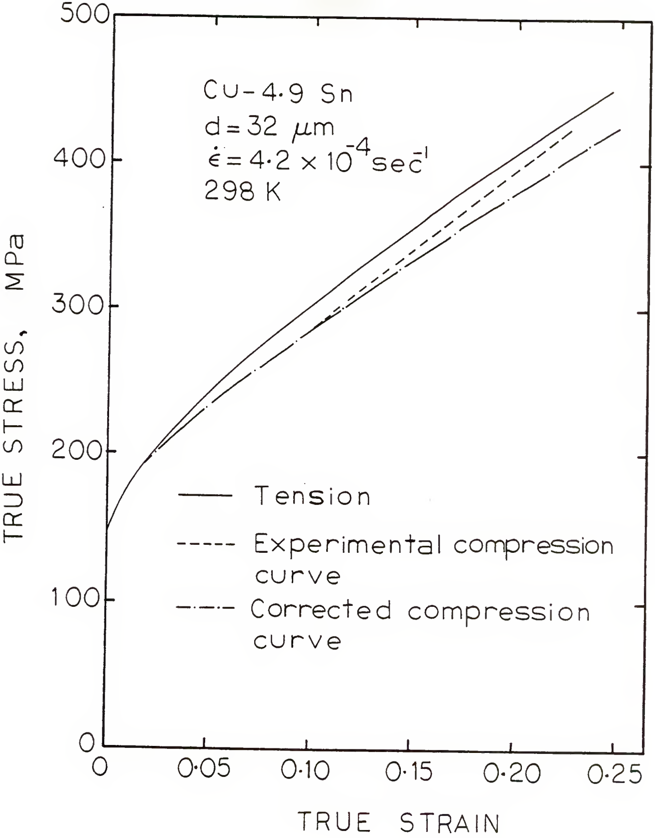
Cu-4.9 Sn
d = 32 μm
ε̇ = 4.2 × 10⁻⁴ sec⁻¹
298 K
Tension
Experimental compression curve
Corrected compression curve
TRUE STRESS, MPa
TRUE STRAIN
0
100
200
300
400
500
0
0·05
0·10
0·15
0·20
0·25

true strains above 0.10. The 298K tensile stress-strain curve is also shown in this figure for comparison.

The stress-strain results obtained with the other materials which were used were similar to those described above. The room temperature tensile and compressive stress-strain curves for Cu-30 at. pct. Zn and Co-40 at. pct. Ni are shown in Figures 11 and 12, respectively. The compression curve is found to be below the tension curve in each case.

4.2 Microstructural Features and Texture Analysis

The nucleation of mechanical twins was found to occur primarily at grain boundaries with some twins forming at triple points and annealing twin boundaries. This is clearly seen in Figure 13. The mechanical twins appear as thin parallel-sided plates with a thickness of a few microns. Figure 14 shows the transverse section of a Cu-4.9 at. pct. Sn alloy tensile specimen deformed to a true strain of 0.20 at 298K. Mechanical twins can be observed within many grains in this specimen. This photomicrograph also shows that the twin traces make an angle of about 60 degrees with each other indicating that the grains that twin in tension have a <111> direction nearly parallel to the stress axis. The corresponding transverse section of a compression specimen deformed to a true strain of 0.10 is shown in Figure 15. In this case, the twins intersect each other at nearly 90 degrees which conforms to twinning in compression

Figure 11

True stress-true strain curves for Cu-30 at. pct. Zn deformed in tension and compression at 298K. The compression curve (dashed line) lies below the tensile curve (solid line) for true strains above 0.03.

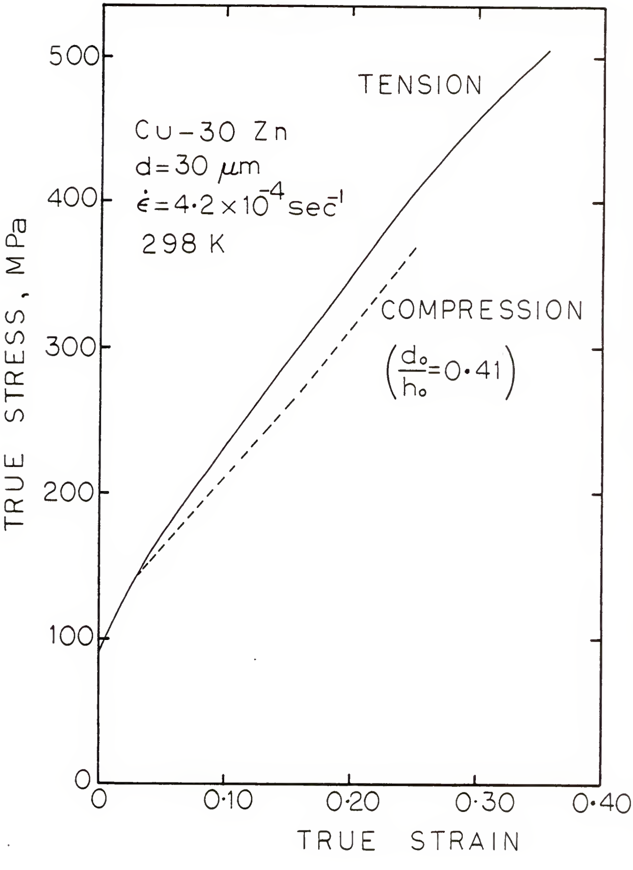
TENSION
Cu-30 Zn
d=30 μm
$\dot{\epsilon}=4\cdot2\times10^{-4}\,sec^{-1}$
298 K
COMPRESSION
$\left(\frac{d_o}{h_o}=0\cdot41\right)$
TRUE STRESS, MPa
TRUE STRAIN
0
100
200
300
400
500
0
0·10
0·20
0·30
0·40

Figure 12

True stress-true strain curves for Co-40 at. pct. Ni tested in tension and compression at 298K. The compression curve (dashed line) lies below the tensile curve (solid line) for true strains above 0.05.

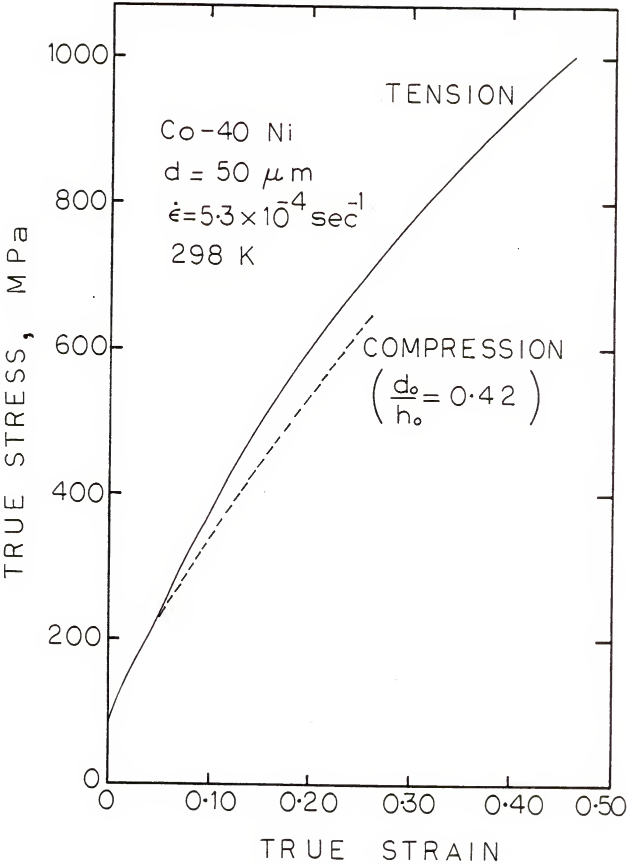
TENSION
Co-40 Ni
d = 50 μm
$\dot{\epsilon}=5.3\times10^{-4}\ \mathrm{sec}^{-1}$
298 K
COMPRESSION
$\left(\frac{d_o}{h_o}=0.42\right)$
TRUE STRESS, MPa
1000
800
600
400
200
0
0
0·10
0·20
0·30
0·40
0·50
TRUE STRAIN

Figure 13

Photomicrograph showing the nucleation of mechanical twins at grain boundaries in a Cu-4.9 at. pct. Sn tensile specimen ($d = 110\ \mu m$) deformed at 298K to a strain of 0.03. Magnification 160 times.

Figure 14

Photomicrograph showing the transverse section of a Cu-4.9 at. pct. Sn specimen (d = 32 μm) deformed in tension to a strain of 0.20 at 298K. The twin traces intersect each other at roughly 60 degrees indicating that the structure which twins in tension has a <111> direction nearly parallel to the stress axis. Magnification 270 times.

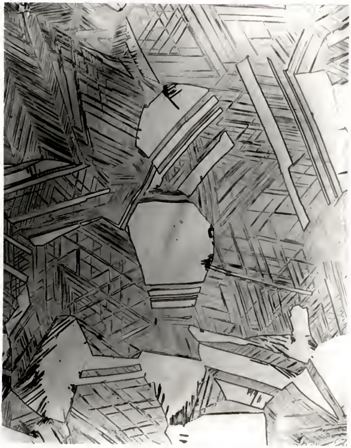

Figure 15

Photomicrograph showing the transverse section of a Cu-4.9 at. pct. Sn specimen (d = 32 μm) deformed in compression to a strain of 0.10 at 298K. The twin traces make an angle of about 90 degrees with each other indicating that the structure twinning in compression has a <100> direction nearly parallel to the stress axis. Magnification 405 times.

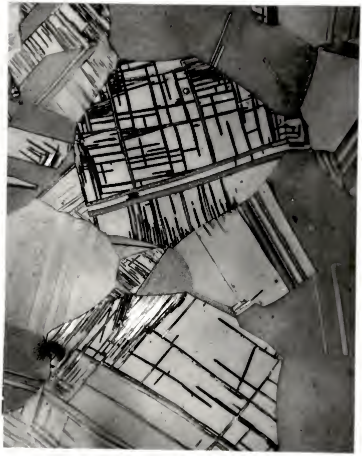

occurring in grains with an orientation near <100>. A pole figure obtained by the quantitative twin trace analysis of 25 grains is shown in Figure 16. Of the 25 grains analyzed in this figure, 15 had orientations within 5 degrees of <111> and 6 grains were near a <100> orientation. The other 4 grains had more general orientations. An additional analysis of the volume fraction of grains which twin in tension and in compression specimens was made by point-counting using a 5 x 5 square grid. Based on the results of all these measurements, it was deduced that the Cu-4.9 at. pct. Sn specimens had a mixed <111>-<100> wire texture with about 65 pct. of the structure close to a <111> orientation, 25 pct. near a <100> orientation and 10 pct. having more general orientations. The low magnification photomicrographs in Figures 17 and 18 illustrate the effects of a mixed texture. Twinning does not occur uniformly in all grains. It is also observed that the number of grains showing twin traces is higher in the tensile sample than in the corresponding compression case.

4.3 The Volume Fraction of Mechanical Twins Formed in Tension and Compression

The microstructures observed at various strains on the transverse sections of tensile specimens deformed at 298K are illustrated in Figures 19 to 22. The microstructures obtained in compression at small strains are shown in Figures 23 and 24. Figure 25 shows the values of V_V^t, the volume fraction of twins, measured in tensile specimens at

Figure 16

Orientation of 25 grains for annealed Cu-4.9 at. pct. Sn alloy with a mean grain intercept of 32 μm. Data were obtained by quantitative trace analysis on a section normal to the stress axis.

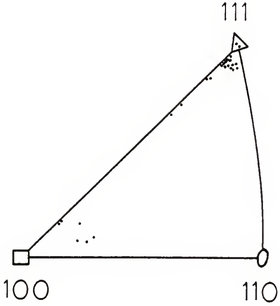
111
100
110

Figure 17

Photomicrograph showing the transverse section of a Cu-4.9 at. pct. Sn alloy tensile specimen (d = 32 μm) deformed to a strain of 0.10 at 298K. Magnification 56 times.

Figure 18

Photomicrograph showing the transverse section of a Cu-4.9 at. pct. Sn compression specimen (d = 32 μm) deformed to a strain of 0.10 at 298K. Magnification 56 times.

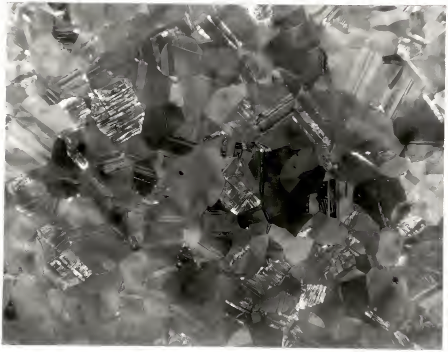

Figure 19

Photomicrograph showing the transverse section of a Cu-4.9 at. pct. Sn specimen (d = 32 μm) deformed in tension to a strain of 0.07 at 298K. Magnification 270 times.

Figure 20

Photomicrograph showing the transverse section of a Cu-4.9 at. pct. Sn specimen (d = 32 μm) deformed in tension to a strain of 0.10 at 298K. Magnification 270 times.

Figure 21

Photomicrograph showing the transverse section of a Cu-4.9 at. pct. Sn specimen (d = 32 μm) deformed in tension to a strain of 0.20 at 298K. Magnification 270 times.

Figure 22

Photomicrograph showing the transverse section of a Cu-4.9 at. pct. Sn specimen (d = 32 μm) deformed in tension to a strain of 0.40 at 298K. Magnification 270 times.

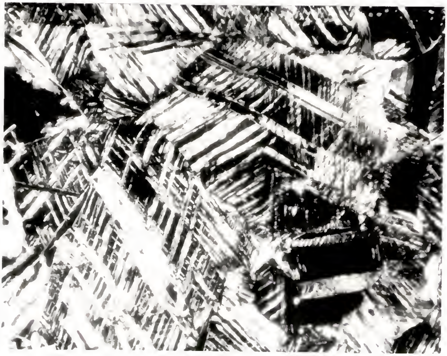

Figure 23

Photomicrograph showing the transverse section of a Cu-4.9 at. pct. Sn specimen (d = 32 μm) deformed in compression to a strain of 0.02 at 298K. Magnification 405 times.

Figure 24

Photomicrograph showing the transverse section of a Cu-4.9 at. pct. Sn specimen (d = 32 μm) deformed in compression to a strain of 0.065 at 298K. Magnification 270 times.

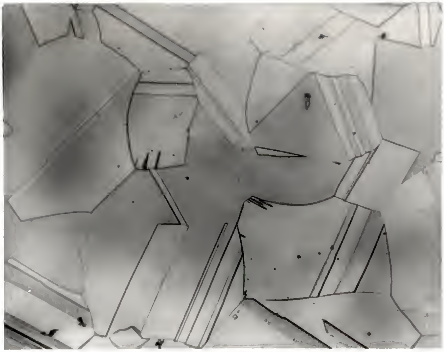

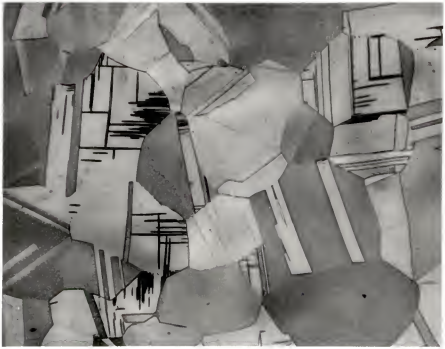

Figure 25

The variation of twinned volume fraction with strain for Cu-4.9 at. pct. Sn deformed in tension at 298K.

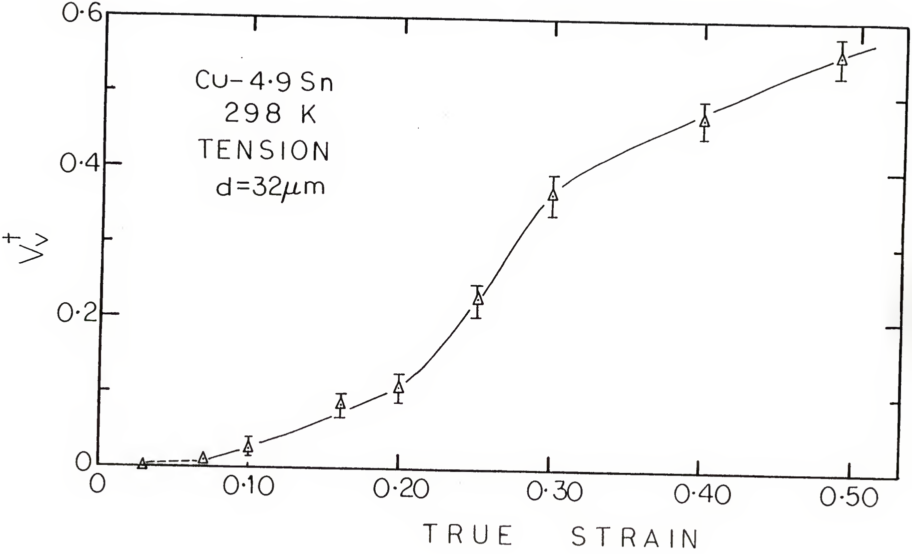

Cu-4·9 Sn
298 K
TENSION
d=32μm
V_V^t
0
0·2
0·4
0·6
0
0·10
0·20
0·30
0·40
0·50
TRUE STRAIN

various true strains up to 0.50. The variation of the twinned volume fraction with strain in tension and compression tests at 298K is shown in Figure 26 for true strains up to about 0.20. Each value of the volume fraction plotted here represents the average of at least 40 measurements. The plots also indicate the 95 pct. confidence intervals for the population mean. The critical strain for the start of twinning was found to be about 0.02 in compression and 0.03 in tension. After a slow start, the volume fraction of twins increases approximately linearly with the true strain in this strain range. Note that within the 0 - 0.20 true strain interval the twinned volume fraction is higher in the compression specimens than in the tension specimens.

4.4 The Microhardness Results

The microhardness data obtained for the twinned and untwinned regions in Cu-4.9 at. pct. Sn compression specimens are shown in Figure 27. The compression specimens were prestrained to various amounts and then sectioned normal to the stress axis. The transverse sections were electropolished and lightly etched to reveal twins in regions with a <100> orientation parallel to the stress axis. As expected, the microhardness was found to increase with increasing prestrain for both twinned and untwinned regions. Further, except at small prestrains, the twinned regions were found to be harder than the regions without twins as indicated in Figure 27.

Figure 26

The variation of twinned volume fraction with strain for Cu-4.9 at. pct. Sn deformed in tension and compression at 298K. The volume fraction of twins is higher in the compression specimens than in the tensile specimens.

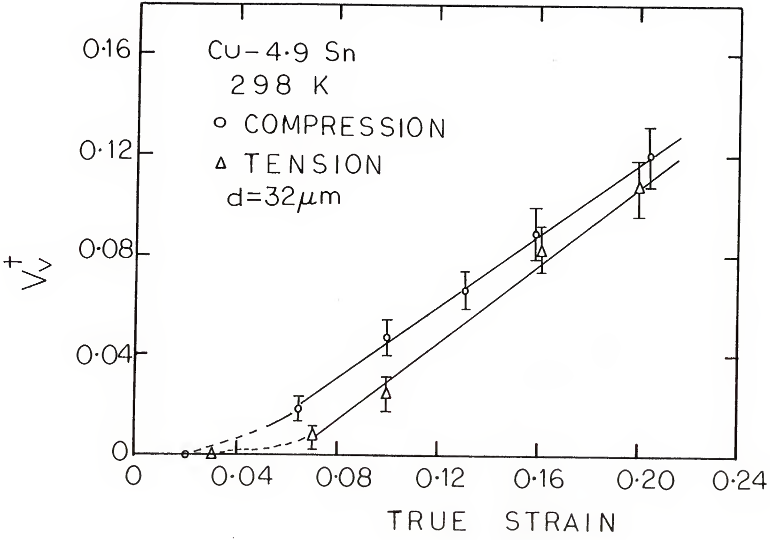
Cu-4·9 Sn
298 K
○ COMPRESSION
△ TENSION
d=32μm
V_v^+
0
0·04
0·08
0·12
0·16
0
0·04
0·08
0·12
0·16
0·20
0·24
TRUE STRAIN

Figure 27

Hardness as a function of compression strain for Cu-4.9 at. pct. Sn (d = 110 μm). Initially, the <100> component has a lower hardness than the <111> component. At higher strains, however, the <100> twinned regions are harder than the untwinned <111> structure.

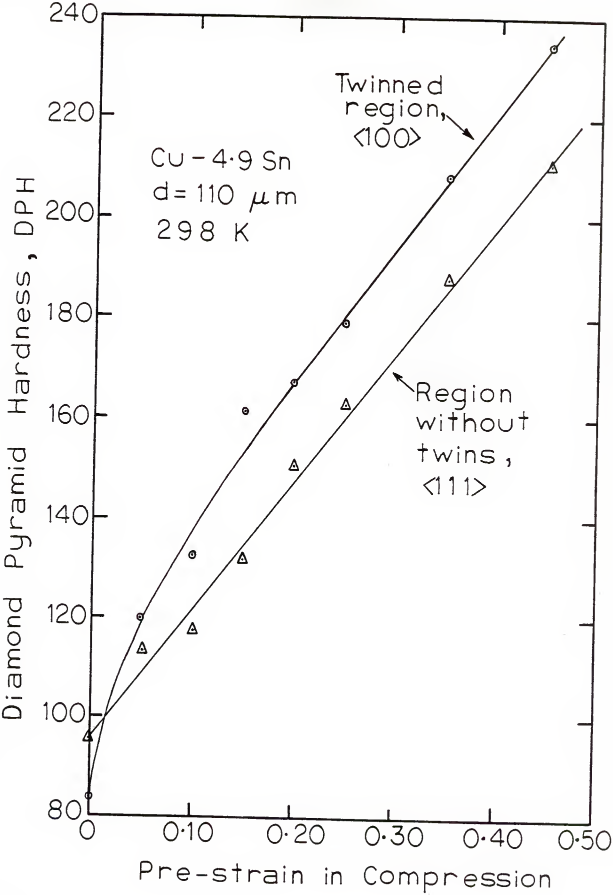
Cu - 4·9 Sn
d = 110 μm
298 K
Twinned region, <100>
Region without twins, <111>
Diamond Pyramid Hardness, DPH
Pre-strain in Compression
80
100
120
140
160
180
200
220
240
0
0·10
0·20
0·30
0·40
0·50

4.5 The Effect of Mean Grain Intercept on Twinning

The tensile stress-strain data obtained for Cu-4.9 at. pct. Sn and Cu-3.1 at. pct. Sn alloys with various mean grain intercepts are shown in Figures 28 to 31. Figures 28 and 29 refer to the tests carried out at 298K with the two alloys. The stress-strain curves obtained at 77K are drawn in Figures 30 and 31. These curves indicate that the flow stress is largely determined by the initial mean intercept. The true stress-true strain curves are shifted to higher stress values as the mean grain intercept is decreased. The total strain obtained is found to be nearly independent of the mean intercept. The stress-strain curves are parabolic at 298K. The curves tend to become nearly linear over a considerable range of strain when the deformation temperature is lowered to 77K. Thus, higher work-hardening rates are observed at the lower temperatures. In both the alloys, the total strain is increased by decreasing the test temperature from 298 to 77K. In order to determine the influence of initial mean intercept on the twinning process, Cu-4.9 at. pct. Sn alloy specimens with various mean grain intercepts were deformed to a true strain of 0.25 at 298K. The specimens were sectioned transverse to the tensile axis and the volume fraction of twins in each sample was measured by point-counting. The values of the twinned volume fraction are plotted against the mean grain intercept in Figure 32. The error bars indicate 95 pct. confidence intervals. This

Figure 28

True stress-true strain curves for Cu-4.9 at. pct. Sn tensile specimens with various mean grain intercepts at 298K.

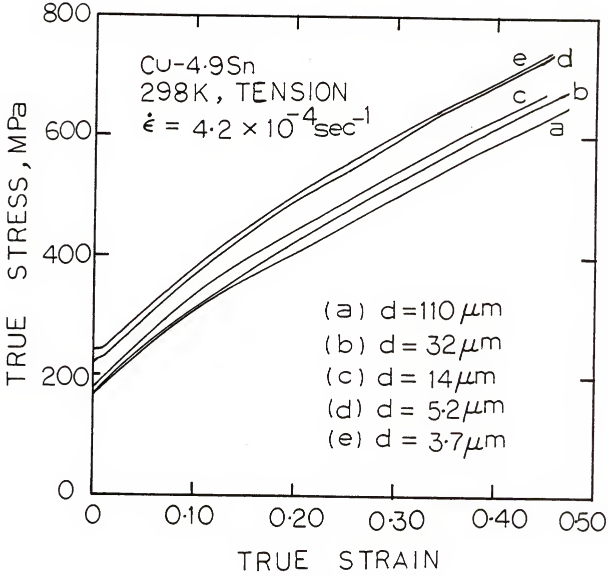
Cu-4·9Sn
298K, TENSION
$\dot{\epsilon} = 4{\cdot}2 \times 10^{-4}\,\mathrm{sec}^{-1}$
TRUE STRESS, MPa
TRUE STRAIN
0
200
400
600
800
0·10
0·20
0·30
0·40
0·50
a
b
c
d
e
(a) d = 110 μm
(b) d = 32 μm
(c) d = 14 μm
(d) d = 5·2 μm
(e) d = 3·7 μm

Figure 29

True stress-true strain curves for Cu-3.1 at. pct. Sn tensile specimens with various mean grain intercepts at 298K.

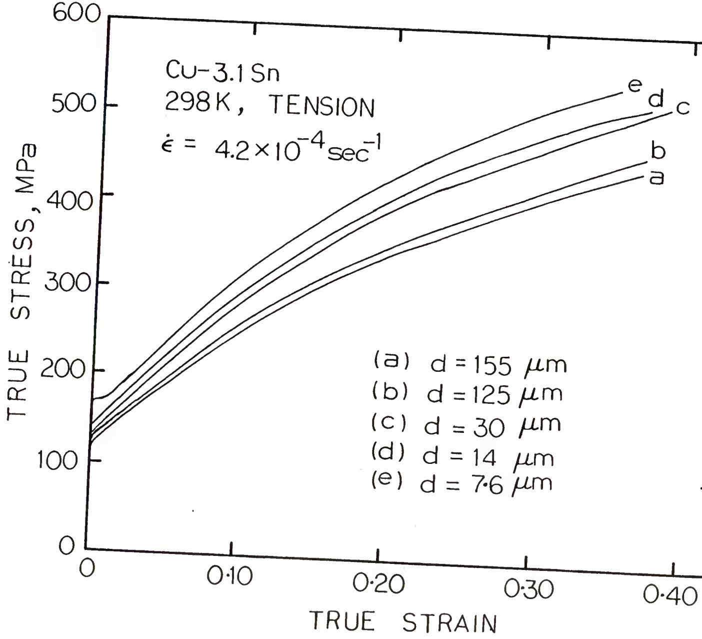
Cu-3.1 Sn
298K, TENSION
$\dot{\epsilon} = 4.2\times10^{-4}\mathrm{sec}^{-1}$
(a) d = 155 μm
(b) d = 125 μm
(c) d = 30 μm
(d) d = 14 μm
(e) d = 7·6 μm
e
d
c
b
a
TRUE STRESS, MPa
0
100
200
300
400
500
600
TRUE STRAIN
0
0·10
0·20
0·30
0·40

Figure 30

True stress-true strain curves for Cu-4.9 at. pct. Sn tensile specimens with various mean grain intercepts at 77K.

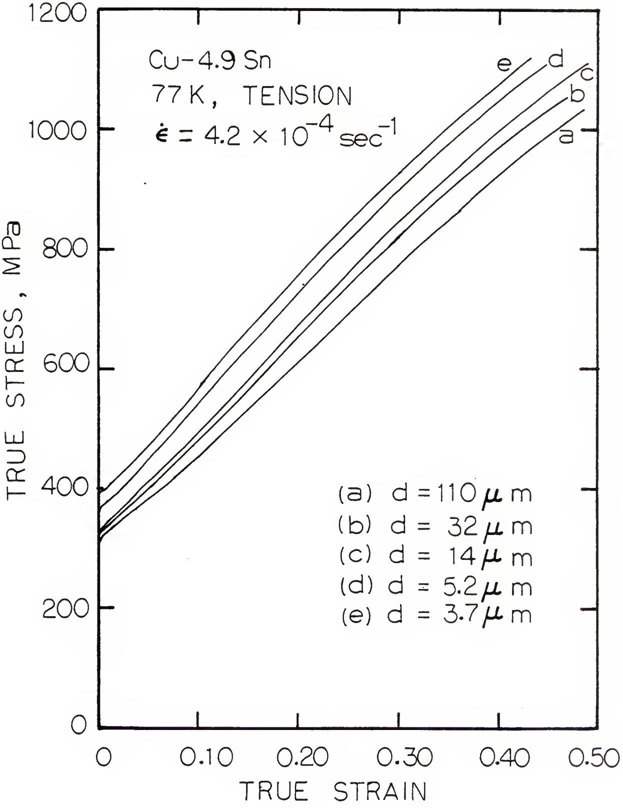
Cu-4.9 Sn
77 K, TENSION
$\dot{\epsilon} = 4.2 \times 10^{-4} sec^{-1}$
TRUE STRESS, MPa
TRUE STRAIN
0
200
400
600
800
1000
1200
0.10
0.20
0.30
0.40
0.50
a
b
c
d
e
(a) d = 110 μm
(b) d = 32 μm
(c) d = 14 μm
(d) d = 5.2 μm
(e) d = 3.7 μm

Figure 31

True stress-true strain curves for Cu-3.1 at. pct. Sn tensile specimens with various mean grain intercepts at 77K.

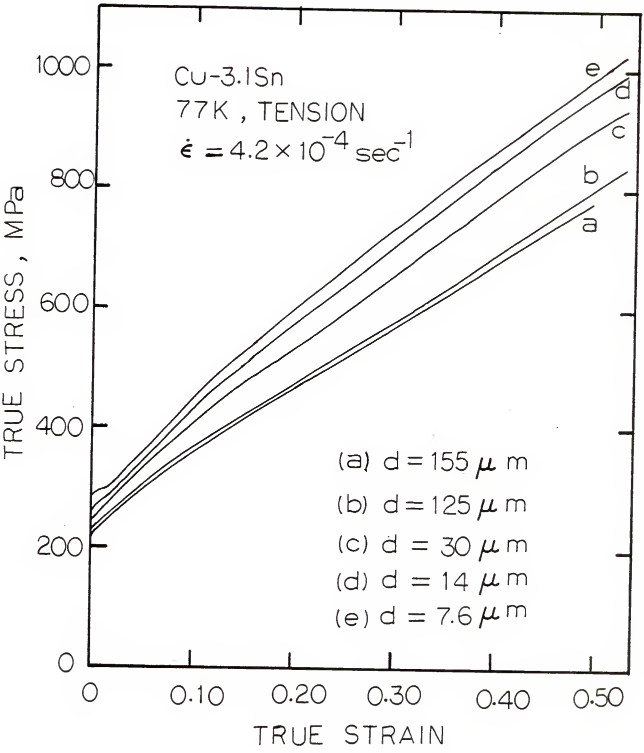
Cu-3.1Sn
77K , TENSION
$\dot{\epsilon} = 4.2 \times 10^{-4}$ sec^{-1}
TRUE STRESS , MPa
1000
800
600
400
200
0
0
0.10
0.20
0.30
0.40
0.50
TRUE STRAIN
e
d
c
b
a
(a) d = 155 μ m
(b) d = 125 μ m
(c) d = 30 μ m
(d) d = 14 μ m
(e) d = 7.6 μ m

Figure 32

The variation of twinned volume fraction with the mean grain intercept for Cu-4.9 at. pct. Sn tensile specimens deformed to a strain of 0.25 at 298K.

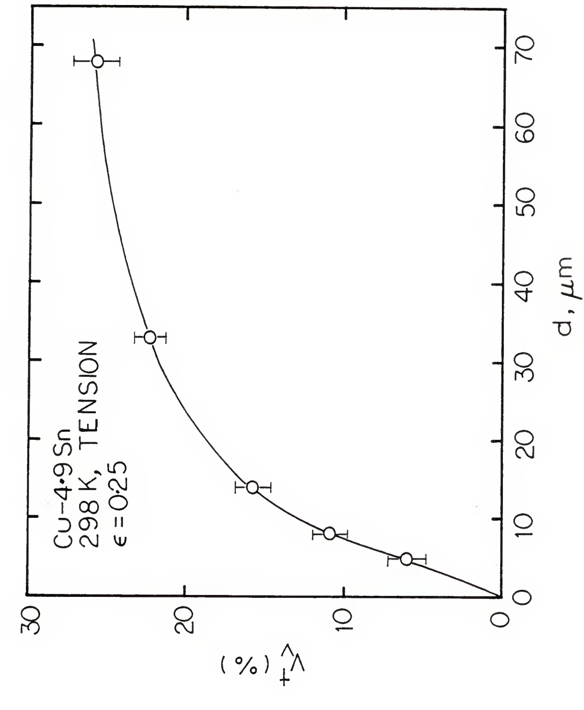
Cu-4·9 Sn
298 K, TENSION
ε = 0·25
$\langle V_t \rangle$ (%)
0
10
20
30
d, μm
0
10
20
30
40
50
60
70

plot shows that the volume fraction of twins increases as the mean grain intercept is increased. The value of the volume fraction tends to level off at large intercepts.

4.6 The Temperature Dependence of Mechanical Twinning

Another characteristic of twinning becomes evident when the mean grain intercept is held constant and the deformation temperature is varied. Tension tests were conducted at several temperatures in the range from 77 to 673K using Cu-3.1 at. pct. Sn alloy specimens with a mean grain intercept of 50 μm. The true stress-true strain curves at five different temperatures are shown in Figure 33. It should be noted that the stress-strain curves are parabolic at high deformation temperatures whereas linear regions are observed at low temperatures. Both work-hardening rate and uniform strain are found to increase as the test temperature is decreased. The dependence of the uniform strain on test temperature is indicated in Figure 34. This figure also shows the variation of the volume fraction of twins with deformation temperature. These volume fraction values were measured by using sections of tensile specimens which had been deformed up to the maximum load at each test temperature. It is observed that the twinned volume fraction in the uniform gage section decreases with increasing deformation temperature.

Figure 33

True stress-true strain curves for Cu-3.1 at. pct. Sn (d = 50 μm) tested in tension at various temperatures.

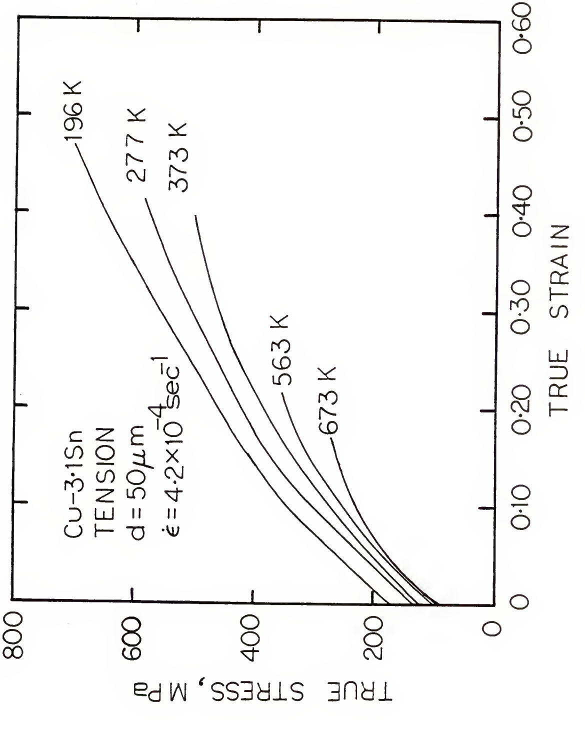
Cu-3·1Sn
TENSION
d = 50μm
ε̇ = 4·2×10⁻⁴ sec⁻¹
196 K
277 K
373 K
563 K
673 K
TRUE STRESS, M Pa
0
200
400
600
800
TRUE STRAIN
0
0·10
0·20
0·30
0·40
0·50
0·60

Figure 34

The variation of uniform strain (ε_u) and twinned volume fraction with test temperature for Cu-3.1 at. pct. Sn (d = 50 μm) deformed in tension.

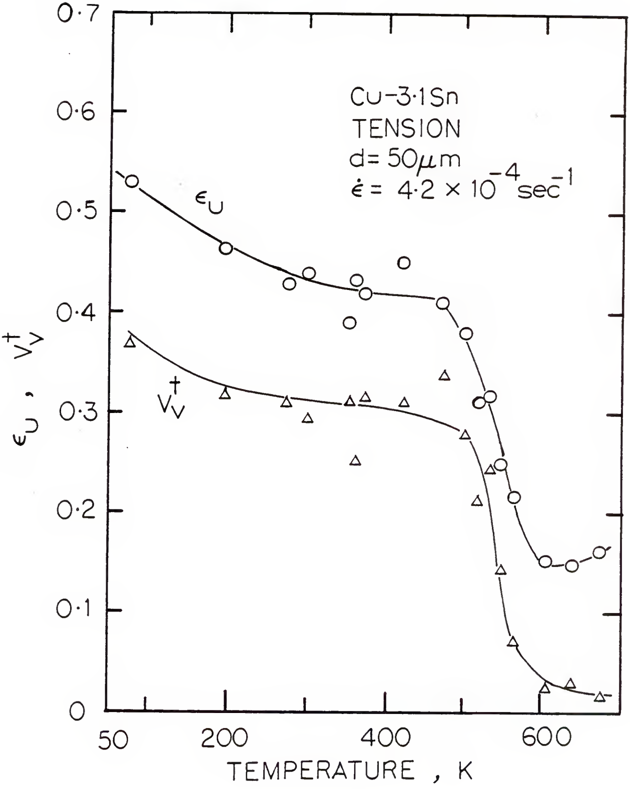
Cu-3·1Sn
TENSION
d= 50μm
$\dot{\epsilon} = 4{\cdot}2 \times 10^{-4}\,sec^{-1}$
ϵ_U
$V_V^\dagger$
ϵ_U , $V_V^\dagger$
0·7
0·6
0·5
0·4
0·3
0·2
0·1
0
50
200
400
600
TEMPERATURE , K

CHAPTER 5
DISCUSSION

5.1 The Stress-Strain Behavior in Tension and Compression

The differences in the tensile and compressive stress-strain curves of Cu-4.9 at. pct. Sn specimens will now be considered. The wire texture of this material is basically a mixture of grains with orientations close to <111> and <100> which is typical of that normally observed in face-centered cubic metals.[36] In the present specimens the duplex <111>-<100> characteristic of the texture is largely associated with the presence of annealing twins. Thus, a grain with an exact <111> orientation will have annealing twins with an orientation of <511> which lies 15.8 degrees from <100>. That twinning in tension specimens occurs first in the 65 pct. volume fraction with a <111> orientation is in good agreement with the fact that the Schmid factor for twinning in tension is larger in a <111> grain by a factor of 1.3 than it is in a <100> grain as may be seen in Table I. On the other hand, in compression, the 25 pct. volume fraction of the structure with a <100> orientation has a near ideal Schmid factor of 0.47 while the <111> component has a Schmid factor of only 0.16. Therefore, twinning in compression is confined primarily to regions with a <100> orientation.

TABLE I

Schmid Factors for Twinning Under Tension and Compression in Grains with [111] or [100] Parallel to the Stress Axis

Orientation	Twinning Schmid Factors	
	Tension	Compression
[111]	0.31	0.16
[100]	0.24	0.47

As noted earlier, the compressive stress-strain curves lie below the tensile curves (Figure 8). This is probably due to the fact that the twinned volume fraction is higher in compression than in tension and that the Schmid factor for twinning of the <100> component of the structure in compression is 0.47 whereas it is only 0.31 for the twinning of <111> component in tension. Both of these factors should make the strain component due to twinning larger in compression than in tension. This hypothesis was tested by using the room temperature stress-strain data for Cu-4.9 at. pct. Sn alloy specimens with a mean grain intercept of 32 μm. It should be recalled that in this material the experimental compression stress-strain curve was corrected for barreling by the extrapolation method (Figure 10). Quantitatively, ε_t, the true strain component due to twinning can be calculated using the equation[37]

$$\varepsilon_t = \phi \gamma V_v^t$$

where ϕ is the Schmid factor for twinning, γ is the twinning shear (0.707) and V_v^t is the volume fraction of twins. If one calculates the twinning strain ε_t using the values of V_v^t in Figure 26 and the Schmid factors in Table I and subtracts it from the total strain of both the tensile and compressive data, then the tensile and compressive curves can be made to coincide as shown in Figure 35. Since the compressive and tensile true stress-true strain curves for face-centered cubic materials are expected to coincide when

Figure 35

True stress-true strain curves for Cu-4.9 at. pct. Sn alloy (d = 32 μm) at 298K. The tension and compression curves nearly coincide if the twinning strain is subtracted from the total strain.

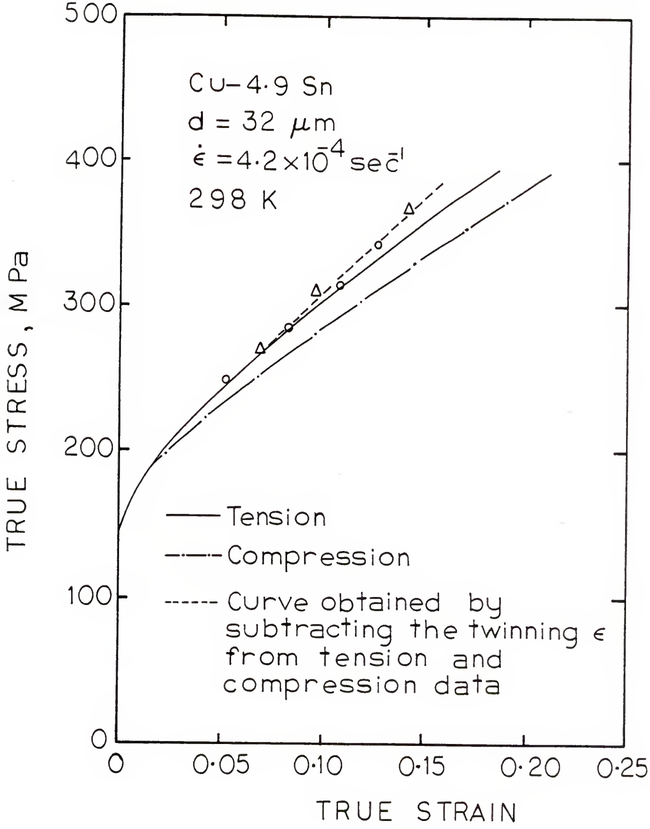
Cu-4·9 Sn
d = 32 μm
ε̇ = 4·2×10⁻⁴ sec⁻¹
298 K
Tension
Compression
Curve obtained by subtracting the twinning ε from tension and compression data
TRUE STRESS, MPa
TRUE STRAIN
0
100
200
300
400
500
0·05
0·10
0·15
0·20
0·25

deformation occurs by slip alone, the present results indicate that the observed difference between tensile and compressive stress-strain curves at strains less than 0.20 can be explained in terms of a difference in the respective strain components due to mechanical twinning. The tension and compression test results obtained for Cu-30 at. pct. Zn and Co-40 at. pct. Ni alloys (Figures 11 and 12) may also be rationalized in a similar manner.

5.2 Effect of Twinning on Work-Hardening Rate

Vöhringer's work[28] on polycrystalline Cu-4.9 at. pct. Sn alloy has shown that when twinning starts, there is a decrease in the work-hardening rate. An analysis of Vöhringer's data revealed a mistake in his $d\varepsilon/d\sigma$ versus σ plots. The ordinate in his plots is not $d\varepsilon/d\sigma$ but it is a mixed variable, $de/d\sigma$, where e is the engineering strain and σ is the true stress. It is important to note this error since $de/d\sigma$ is not a correct measure of the reciprocal of the work-hardening rate. The values of $de/d\sigma$ and $d\varepsilon/d\sigma$ are very close to each other at small strains. However, these two variables differ significantly at large strains. Figure 36 shows Vöhringer's plot of $de/d\sigma$ versus σ for a specimen with a mean grain intercept of 200 μm. The start of twinning is accompanied by a sharp upward inflection (shown by the arrow) in the $de/d\sigma$ versus σ curve. A corresponding $de/d\sigma$ versus σ curve obtained in the present work for a tensile specimen having a mean grain intercept

Figure 36

The variation of $de/d\sigma$ and $d\varepsilon/d\sigma$ with σ for Cu-4.9 at. pct. Sn tensile specimens. Vöhringer's results are compared with the present data. The arrows indicate the start of twinning.

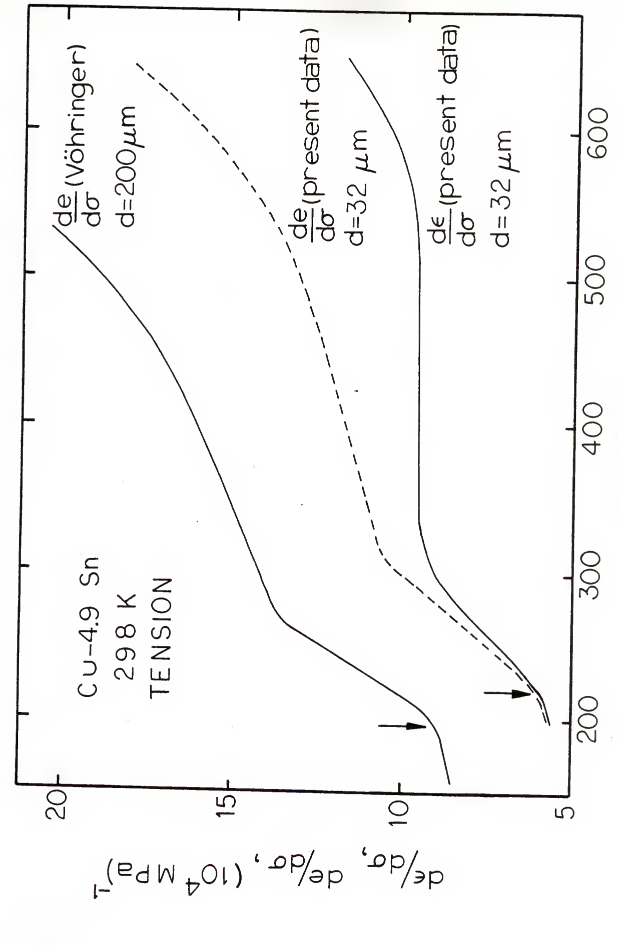
Cu-4.9 Sn
298 K
TENSION
$\frac{de}{d\sigma}$ (Vöhringer)
d=200 μm
$\frac{de}{d\sigma}$ (present data)
d=32 μm
$\frac{d\epsilon}{d\sigma}$ (present data)
d=32 μm
σ , MPa
200
300
400
500
600
5
10
15
20
dε/dσ, de/dσ, (10^4 MPa$)^{-1}$

of 32 μm is given in Figure 36 below Vöhringer's curve. Note that this curve is similar to Vöhringer's. Furthermore, the upward inflection in the present data coincided with the start of twinning. This inflection is seen clearly if the $d\varepsilon/d\sigma$ versus σ curve is plotted in its entirety as will be shown later. The present results concerning the start of twinning are thus in agreement with Vöhringer's observations. Vöhringer proposed that the increase in $de/d\sigma$, or a decrease in $d\sigma/de$, can be accounted for by assuming that the formation of a twin adds an increment to the strain but does not affect the flow stress. Briefly, this would have the effect of decreasing the work-hardening rate once twinning begins. This hypothesis lends support to the observed differences between tensile and compressive stress-strain curves. However, the role of twinning in the development of the stress-strain curves of polycrystalline face-centered cubic metals is still unresolved. An alternative point of view has been suggested by Rémy[31] who has worked on Co-33 wt. pct. Ni. According to Rémy,[31] twinning should increase the flow stress due to the fact that the twin boundaries increase the total boundary area per unit volume. Thus, the effect of twinning should be to increase the work-hardening rate and not decrease it as suggested by Vöhringer. Another feature of Rémy's analysis is that he assumes that once a twin forms, slip ceases inside the twinned material so that slip continues only in the ever decreasing volume fraction of untwinned material. This should also act to increase the macroscopic work-hardening rate.

It was previously assumed that this difference of opinion between Rémy and Vöhringer on how twinning influences the work-hardening in low stacking fault energy face-centered cubic metals may be due to a difference in the materials that were investigated since Rémy used a Co-Ni alloy and Vöhringer employed copper based alloys. According to Rémy,[31] his $d\varepsilon/d\sigma$ versus σ curves did not show a typical inflection corresponding to a lowering of the work-hardening rate at the start of twinning. But he has not reported his $d\varepsilon/d\sigma$ versus σ data for Co-Ni alloys. The test results obtained for Co-40 at. pct. Ni specimens in the present investigation were used to verify Remy's statement. The $d\varepsilon/d\sigma$ versus σ plot for Co-40 at. pct. Ni deformed in tension is shown in Figure 37. An upward inflection corresponding to the start of twinning is evident at the region indicated by the arrow "a."

Vöhringer concluded that the effect of mechanical twins is to decrease the work-hardening rate. His conclusion was based on the observation that $de/d\sigma$ increased continuously with σ. However, $d\varepsilon/d\sigma$ rather than $de/d\sigma$ represents the reciprocal of the work-hardening rate. Consider the lowest curve in Figure 36 where $d\varepsilon/d\sigma$ is plotted versus σ. This curve is drawn separately in Figure 38 by including the variation of $d\varepsilon/d\sigma$ with σ in the post-yield region. This figure shows that $d\varepsilon/d\sigma$ levels off after an initial rise at

Figure 37

The variation of $d\varepsilon/d\sigma$ with σ for a Co-40 at. pct. Ni ($d = 50$ μm) tensile specimen tested at 298K. The arrows correspond to the microstructures shown in Figures 39 to 42.

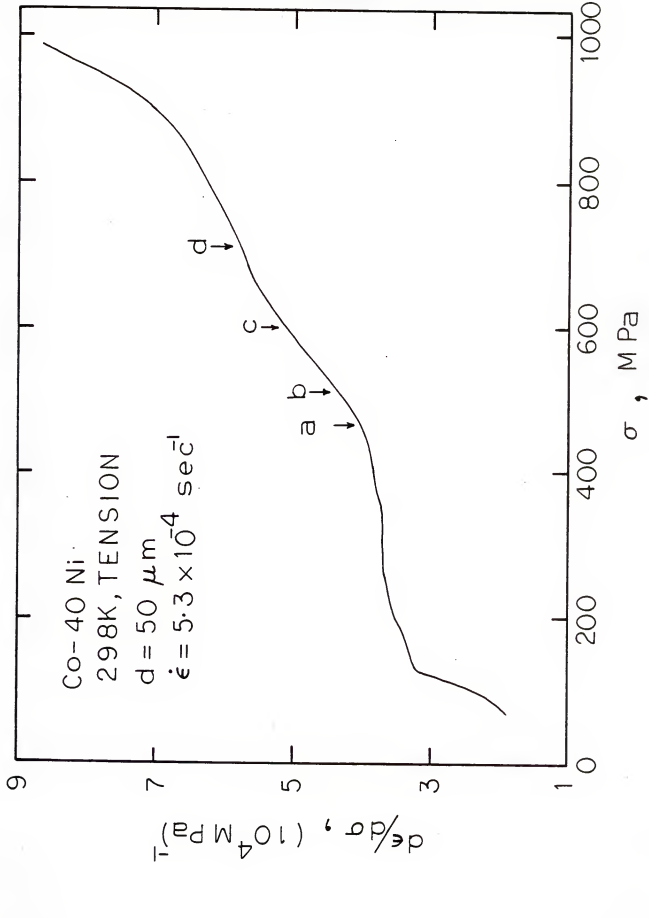
Co- 40 Ni
298K, TENSION
d = 50 μm
$\dot{\epsilon} = 5.3 \times 10^{-4}$ sec^{-1}
a
b
c
d
$d\epsilon/d\sigma$, (10^4 M Pa)$^{-1}$
1
3
5
7
9
σ , M Pa
0
200
400
600
800
1000

Figure 38

The variation of $d\varepsilon/d\sigma$ with σ for a Cu-4.9 at. pct. Sn tensile specimen ($d = 32$ µm) at 298K. The arrow "a" represents the start of twinning. The arrows "b" to "e" correspond to the microstructures shown in Figures 19 to 22.

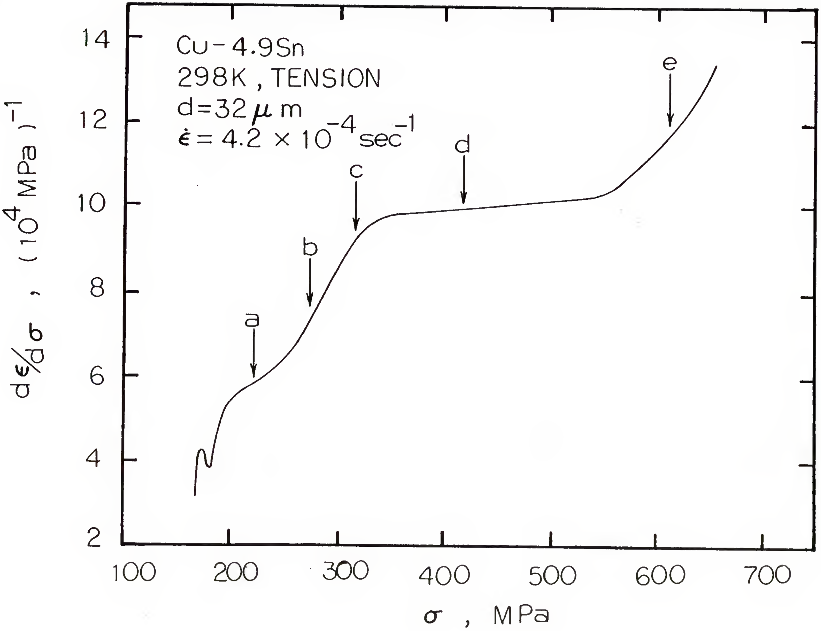
Cu-4.9Sn
298K, TENSION
d=32 μm
$\dot{\epsilon} = 4.2 \times 10^{-4}\,sec^{-1}$
a
b
c
d
e
$d\epsilon/d\sigma$, $(10^4\,MPa)^{-1}$
2
4
6
8
10
12
14
100
200
300
400
500
600
700
σ , MPa

"a" and remains nearly constant beyond "c" over a considerable range of the stress-strain curve. In other words, the work-hardening rate actually reaches a constant value instead of decreasing continuously as implied by the de/dσ versus σ curve. This is also evident from the linear region of the stress-strain curve (Figure 8).

5.3 The Role of Microstructural Changes

A metallographic study of the development of the twinned structure with increasing strain supports the conclusion that there is a change in the role that the twins have on the work-hardening characteristics as the strain increases. Consider the dε/dσ versus σ plot shown in Figure 38 for the tensile deformation of a Cu-4.9 at. pct. Sn alloy specimen with a mean grain intercept of 32 μm. The arrows at "b," "c," "d" and "e" indicated on this curve correspond to the microstructures shown in Figures 19 to 22, respectively. Twin nucleation occurs at "a" and this gives rise to the observed inflection. At "b" and "c," the microstructures corresponding to strains of 0.07 and 0.10 (Figures 19 and 20) show that initially the twins tend to be parallel and form largely on one crystallographic plane in any given region of the structure. Previous investigations[21,38-40] using single crystals have shown that there is a strong correlation between the most active slip plane and the twinning plane in face-centered cubic metals. Thus, the initial twinning should not strongly influence slip and the work-hardening. On the other hand, twins form on intersecting planes at larger strains indicated by arrows "d" and "e" in Figure 38. This can be seen in Figures 21 and 22 which show the microstructures of specimens deformed to strains of 0.20 and 0.40, respectively. The tendency for twins to form on intersecting planes at large strains should have the effect of increasing the flow stress due to the subdivision of structure.

The microstructural changes in the Co-40 at. pct. Ni tensile specimens were similar to those in Cu-4.9 at. pct. Sn alloy. The variation of $d\varepsilon/d\sigma$ with σ for Co-40 at. pct. Ni was shown in Figure 37. In this figure the arrows shown at "a," "b," "c" and "d" correspond to the specimens that were examined metallographically. The microstructures observed in these specimens are shown in Figures 39 to 42, respectively. The rise in $d\varepsilon/d\sigma$ at "a" correlates with the nucleation of twins. At "b," the twins are still parallel to each other in any given region of the structure. Twins are observed on intersecting planes when the samples are deformed up to "c" and "d." These results agree with the lower rate of increase of $d\varepsilon/d\sigma$ beyond "c" and "d."

While the influence of twinning on the work-hardening rate is similar in Cu-4.9 at. pct. Sn and Co-40 at. pct. Ni alloys, there is a considerable difference between the $d\varepsilon/d\sigma$ versus σ plots of these two materials. In Cu-4.9 at. pct. Sn (Figure 38), the upward inflection corresponding to twin nucleation occurs much earlier. Also, in this alloy,

Figure 39

Photomicrograph showing the transverse section of a Co-40 at. pct. Ni tensile specimen (d = 50 μm) deformed at 298K to a true strain of 0.14 (corresponding to the arrow "a" in Figure 37). Magnification 160 times.

Figure 40

Photomicrograph showing the transverse section of a Co-40 at. pct. Ni tensile specimen (d = 50 μm) deformed at 298K to a true strain of 0.16 (corresponding to the arrow "b" in Figure 37). Magnification 160 times.

Figure 41

Photomicrograph showing the transverse section of a Co-40 at. pct. Ni tensile specimen (d = 50 μm) deformed at 298K to a true strain of 0.20 (corresponding to the arrow "c" in Figure 37). Magnification 160 times.

Figure 42

Photomicrograph showing the transverse section of a Co-40 at. pct. Ni tensile specimen (d = 50 μm) deformed at 298K to a true strain of 0.27 (corresponding to the arrow "d" in Figure 37). Magnification 160 times.

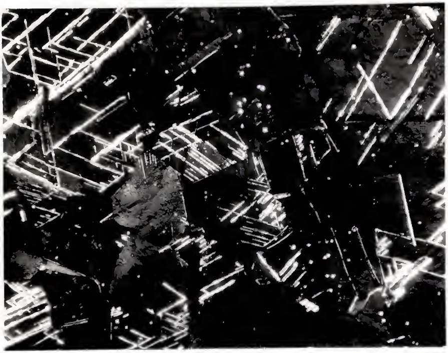

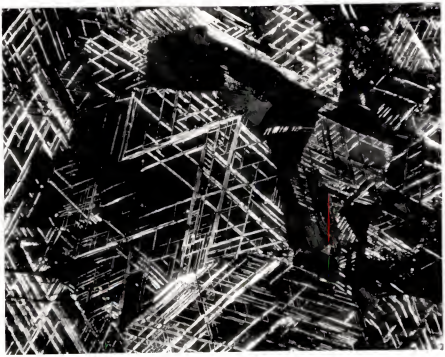

there is a range where $d\varepsilon/d\sigma$ is nearly constant. This implies that the stress-strain curve is linear over a range of strains. However, no such range is found in the case of Co-40 at. pct. Ni (Figure 37). In this alloy, the twin nucleation occurs later and $d\varepsilon/d\sigma$ does not remain constant over some range of strains beyond "d."

An interesting result is obtained when a plot of $d\varepsilon/d\sigma$ versus σ is made for Cu-3.1 at. pct. Sn deformed in tension at 298K. This variation, shown in Figure 43, appears to be very similar to the $d\varepsilon/d\sigma$ versus σ plot for Co-40 at. pct. Ni. It should be noted that both these alloys start to twin after a considerable amount of slip deformation. Furthermore, there is no region of constant work-hardening rate in both cases. Thus, the stress-strain curves for these two materials are qualitatively similar. This is due to a similar value of the stacking fault energy (24 $mJ \cdot m^{-2}$) in these two alloys, one that is roughly twice that in the Cu-4.9 at. pct. Sn composition.[29,41]

The changes in the slope of $d\varepsilon/d\sigma$ versus σ plot of Cu-3.1 at. pct. Sn shown in Figure 43 agree well with the microstructures observed at "a," "b" and "c" as can be seen in Figures 44 to 46. Therefore, the role of microstructural changes appears to be very similar in all the cases which have been considered. In all the polycrystalline materials that were examined there are distinct stages in the $d\varepsilon/d\sigma$ versus σ curves. The nucleation of twins causes a drop in the work-hardening rate as indicated by the

Figure 43

The variation of $d\varepsilon/d\sigma$ with σ for a Cu-3.1 at. pct. Sn tensile specimen ($d = 30$ μm) at 298K. The arrows correspond to the microstructures shown in Figures 44 to 46.

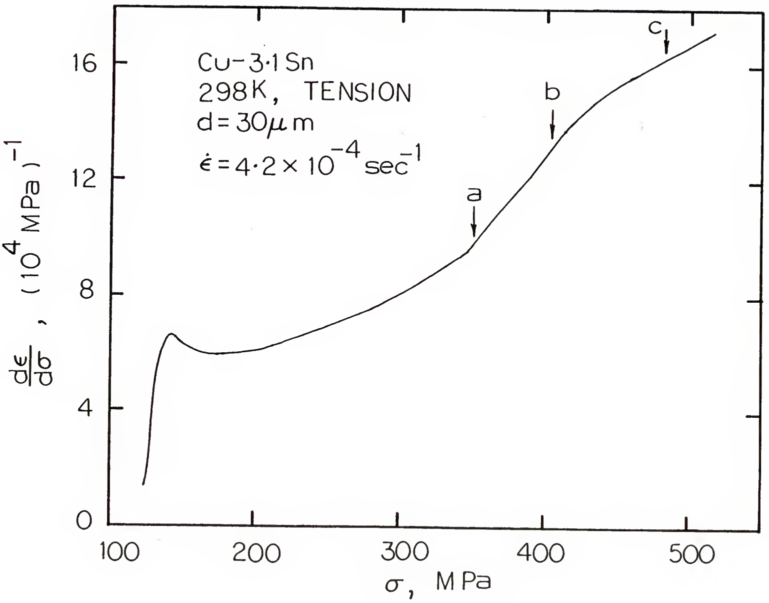
Cu-3·1Sn
298K, TENSION
d=30μm
$\dot{\epsilon}=4{\cdot}2\times10^{-4}\,\mathrm{sec}^{-1}$
a
b
c
$\frac{d\epsilon}{d\sigma}$, $(10^4\,\mathrm{MPa})^{-1}$
0
4
8
12
16
100
200
300
400
500
σ, MPa

Figure 44

Photomicrograph showing the transverse section of a Cu-3.1 at. pct. Sn tensile specimen (d = 30 μm) deformed at 298K to a true strain of 0.18 (corresponding to the arrow "a" in Figure 43). Magnification 270 times.

Figure 45

Photomicrograph showing the transverse section of a Cu-3.1 at. pct. Sn tensile specimen (d = 30 μm) deformed at 298K to a true strain of 0.23 (corresponding to the arrow "b" in Figure 43). Magnification 270 times.

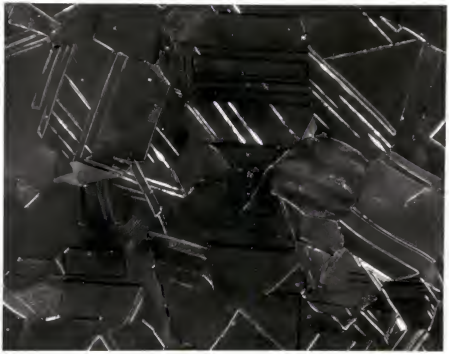

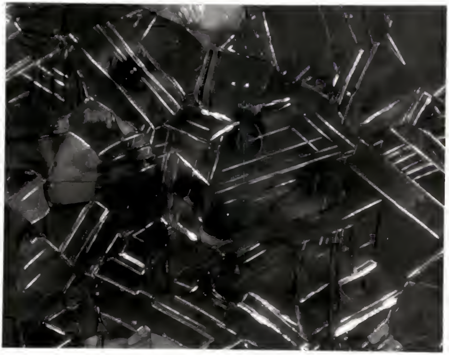

Figure 46

Photomicrograph showing the transverse section of a Cu-3.1 at. pct. Sn tensile specimen (d = 30 μm) deformed at 298K to a true strain of 0.33 (corresponding to the arrow "c" in Figure 43). Magnification 270 times.

upward inflection. However, when twin intersections occur within many grains, the work-hardening rate no longer decreases in the same manner. There is a drop in the rate of decrease of the work-hardening rate. In fact, the work-hardening rate reaches a constant value over a range of the stress-strain curve when the stacking fault energy is low as in the case of Cu-4.9 at. pct. Sn alloy. In other words, the twins forming on intersecting planes at larger strains appear to have a strengthening effect.

The results of Mori and Fujita[40] in their studies of Cu-8 at. pct. Al single crystals lend support to the present observations. During deformation of crystals near the [011] axis, they found that twinning occurred along the primary slip plane before the appearance of the conjugate slip bands. They observed that the activation of primary twinning alone gives rise to a reduction of the work-hardening rate. This is seen as a downward inflection on the stress-strain curve. After the work-hardening rate had decreased by more than 30 pct., a new increase in the work-hardening is observed when conjugate twins are activated. The stress-strain curve exhibits an upward inflection at this stage. Thus, even in single crystals there is evidence of the role of twins as obstacles when there is some interaction between two twinning systems.

5.4 The Microhardness of Twinned and Untwinned Regions

The microhardness data (Figure 27) obtained from the transverse sections of Cu-4.9 at. pct. Sn compression specimens support the hypothesis concerning the role of twinning. In Figure 27, two curves are given showing hardness as a function of compressive prestrain for grains with <100> and <111> orientations, respectively. Although twinning in compression is limited to the grains in the <100> component of the structure, initially this component has a lower hardness than the <111> component. There is a good correlation between hardness and the uniaxial flow stress at about 8 pct. strain.[42,43] Thus, the hardness results cannot be directly correlated to the expected yield stresses for slip in the <100> and <111> grains based on their Schmid factors. (The Schmid factor for slip is 0.41 for the <100> orientation, whereas it is only 0.27 for the <111> component.) However, it is significant that the hardness data are consistent with a lower yield stress of the <100> grains which have a higher Schmid factor for slip. The lower initial hardness of the <100> grains probably results from the fact that at 8 pct. strain the volume fraction of twins is still not large enough to overpower the lower yield condition in the <100> grains. At higher strains, however, the <100> twinned regions become harder than the untwinned regions which supports the conclusion that twinning eventually increases the work-hardening.

The microhardness values obtained by Blicharski and Gorczyca[44] in an austenitic stainless steel provide additional evidence concerning the hardening effect of mechanical twins. This steel was deformed by rolling to various true strains in the range 0.5 to 2.0, and then the hardness was measured by using etched specimens. These authors found that the "etched areas" were significantly harder than the "unetched areas." This again goes to show the strengthening effect of the twins.

5.5 The Role of Deformation Temperature

The influence of temperature on the stress-strain behavior of Cu-4.9 at. pct. Sn and Cu-3.1 at. pct. Sn alloys was shown in Figures 8 and 33, respectively. These results indicate that both the work-hardening rate and the uniform strain are increased by lowering the deformation temperature. Rémy[31] obtained similar stress-strain curves for Co-33 wt. pct. Ni alloy in the temperature range 293 to 573K. He has also reported that the twin nucleation is postponed to higher strains and that the volume fraction of twins is decreased as the test temperature is increased. These results can be used to rationalize the observed temperature dependence of the stress-strain data. The higher work-hardening rate at low temperatures has been attributed to the enhanced twinning deformation.

No attempt was made by the previous investigators to correlate the variation of the work-hardening rate with changes in the microstructure at low temperatures. Vöhringer[29] assumed that the $d\varepsilon/d\sigma$ versus σ plots would be similar to each other at all deformation temperatures. It will now be shown that this is not the case. The $d\varepsilon/d\sigma$ versus σ curve for a Cu-4.9 at. pct. Sn specimen deformed at 77K is shown in Figure 47. A comparison of Figures 38 and 47 reveals that the stress dependence of $d\varepsilon/d\sigma$ is greatly influenced by the deformation temperature. The typical inflection at the start of twinning is absent in the $d\varepsilon/d\sigma$ curve at 77K (Figure 47). The microstructures observed at "a," "b" and "c" are shown in Figures 48 to 50, respectively. Figure 48 shows the mechanical twins nucleating at grain boundaries and triple points in a tensile specimen deformed to a strain of 0.01 at 77K. It should also be noticed that the twin nucleation occurs on more than one plane leading to twin intersections even at this small strain. More and more twins form on intersecting planes as the strain is increased. This is indicated in Figures 49 and 50. This should cause an increase in the work-hardening rate at higher strains. This effect is clearly seen in Figure 47 where the value of $d\varepsilon/d\sigma$ decreases beyond "b." In other words, the work-hardening rate actually increases after this point and approaches a constant value. Beyond this stage, the work-hardening rate remains nearly constant over a range of the stress-strain curve and then decreases again. These results imply that the high work-hardening rates observed at low temperatures in these alloys may be due to the twin

Figure 47

The variation of $d\varepsilon/d\sigma$ with σ for a Cu-4.9 at. pct. Sn tensile specimen ($d = 110$ μm) tested at 77K. The arrows correspond to the microstructures shown in Figures 48 to 50.

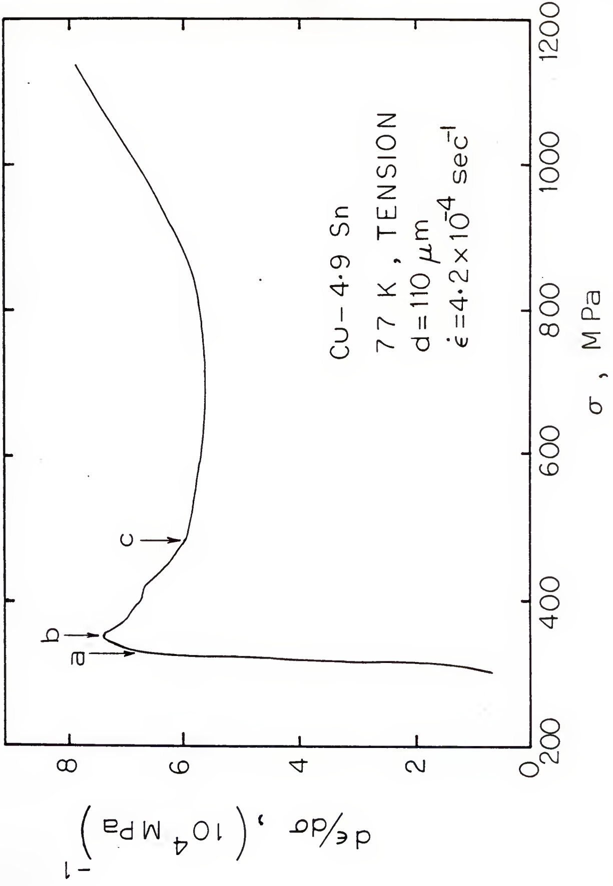
Cu – 4·9 Sn
77 K , TENSION
d = 110 μm
ε̇ = 4·2 × 10⁻⁴ sec⁻¹
a
b
c
dε/dσ , (10⁴ MPa)⁻¹
0
2
4
6
8
200
400
600
800
1000
1200
σ , MPa

Figure 48

Photomicrograph showing the transverse section of a Cu-4.9 at. pct. Sn tensile specimen (d = 110 μm) deformed at 77K to a true strain of 0.01 (corresponding to the arrow "a" in Figure 47). Magnification 270 times.

Figure 49

Photomicrograph showing the transverse section of a Cu-4.9 at. pct. Sn tensile specimen (d = 110 μm) deformed at 77K to a true strain of 0.03 (corresponding to the arrow "b" in Figure 47). Magnification 270 times.

Figure 50

Photomicrograph showing the transverse section of a Cu-4.9 at. pct. Sn tensile specimen (d = 110 μm) deformed at 77K to a true strain of 0.11 (corresponding to the arrow "c" in Figure 47). Magnification 270 times.

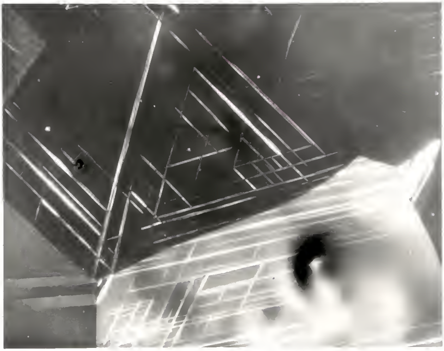

nucleation occurring on more than one plane and the high volume fraction of twins forming at these temperatures.

The temperature dependence of the stress-strain curves of Cu-3.1 at. pct. Sn shown in Figure 33 will now be considered. This dependence is very similar to the results obtained by Carreker[6] in the case of silver. As Figure 34 indicates, the volume fraction of twins increases as the deformation temperature is lowered. This should explain the high values of work-hardening rate and uniform strain observed at low temperatures. It is also seen from Figure 34 that both the twinned volume fraction and the uniform strain vary with test temperature in the same manner. If the uniform strain is plotted as a function of the volume fraction of twins, a direct relation is observed between these two parameters. This is shown in Figure 51. There are two factors that lead to this effect. First, the strain contributed by twinning, ε_t, is directly related to the volume fraction of twins, V_v^t, by the equation[37]

$$\varepsilon_t = \phi \gamma V_v^t$$

where ϕ is the Schmid factor for twinning and γ is the twinning shear. The second contribution to the uniform strain arises due to the indirect effect of increased work-hardening rate which delays plastic instability.

Figure 51

The dependence of uniform strain on twinned volume fraction in Cu-3.1 at. pct. Sn tensile specimens (d = 50 μm).

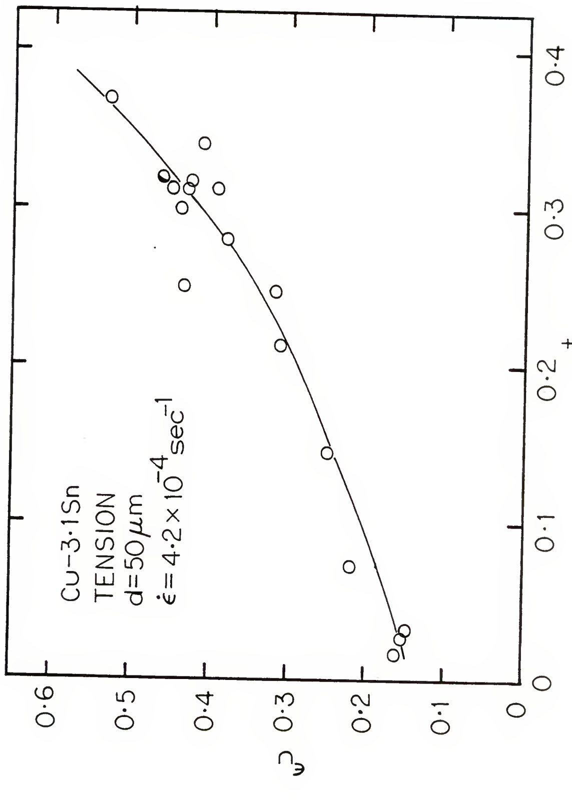
Cu-3·1Sn
TENSION
d=50μm
ε̇ = 4·2×10⁻⁴ sec⁻¹
ε_c
0
0·1
0·2
0·3
0·4
0·5
0·6
0
0·1
0·2
0·3
0·4
V_V^t

5.6 The Role of Initial Boundary Area

It is generally believed that twinning deformation is affected by the initial boundary area. According to the present results shown in Figure 32, the twinned volume fraction V_V^t increases as the mean grain intercept is increased. As expected, the stress-strain curves for Cu-4.9 at. pct. Sn and Cu-3.1 at. pct. Sn alloys with various mean grain intercepts (Figures 28 to 31) indicate that the stress level increases as the mean intercept is decreased. The total elongation is observed to be independent of the mean intercept at any given temperature. In order to understand the variation of the work-hardening rate with changing grain size, the plots of $d\varepsilon/d\sigma$ versus σ were derived from the stress-strain data. The $d\varepsilon/d\sigma$ versus σ plots for the two alloys at 298 and 77K are shown in Figures 52 to 55. Each of these plots will now be considered briefly.

The $d\varepsilon/d\sigma$ versus σ curves for the room temperature deformation of Cu-4.9 at. pct. Sn tensile specimens with mean grain intercepts in the range 3.7 to 110 μm are shown in Figure 52. The curves "a," "b" and "c" for the coarse-grained specimens show the upward inflections corresponding to twin nucleation and the leveling off of $d\varepsilon/d\sigma$ when twin intersections occur in many grains. The fine-grained specimens (curves "d" and "e") show a different variation of $d\varepsilon/d\sigma$ versus σ initially. The $d\varepsilon/d\sigma$ values are initially large in these two cases and there is a sudden drop of

Figure 52

The variation of $d\varepsilon/d\sigma$ with σ for Cu-4.9 at. pct. Sn tensile specimens having various mean grain intercepts at 298K. The circles represent the start of twinning. The triangles represent twin intersections within many grains.

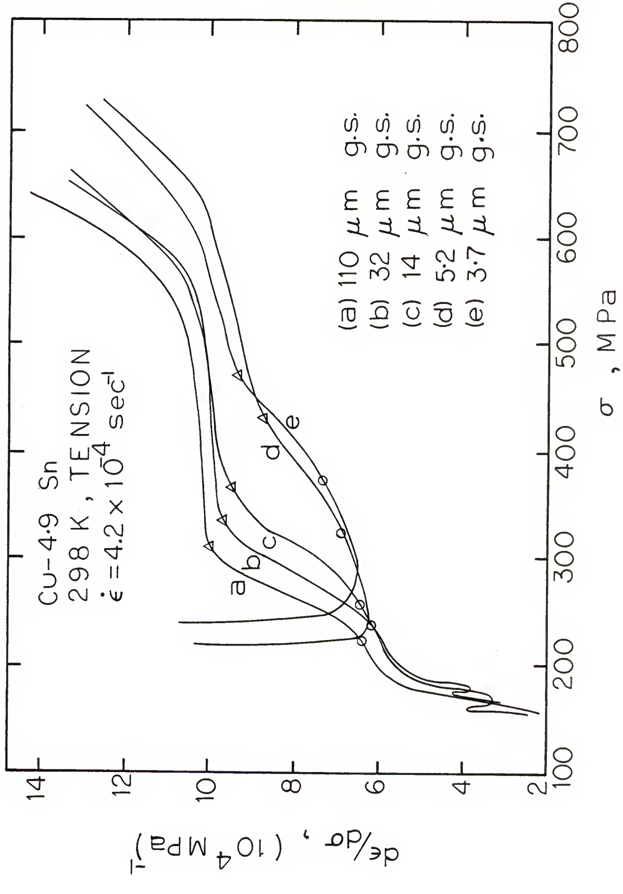
Cu-4.9 Sn
298 K , TENSION
$\dot{\epsilon} = 4.2 \times 10^{-4}$ sec^{-1}
(a) 110 μm g.s.
(b) 32 μm g.s.
(c) 14 μm g.s.
(d) 5.2 μm g.s.
(e) 3.7 μm g.s.
a
b
c
d
e
σ , MPa
100
200
300
400
500
600
700
800
dε/dσ , (10^4 MPa$)^{-1}$
2
4
6
8
10
12
14

Figure 53

The variation of $d\varepsilon/d\sigma$ with σ for Cu-3.1 at. pct. Sn tensile specimens having various mean grain intercepts at 298K.

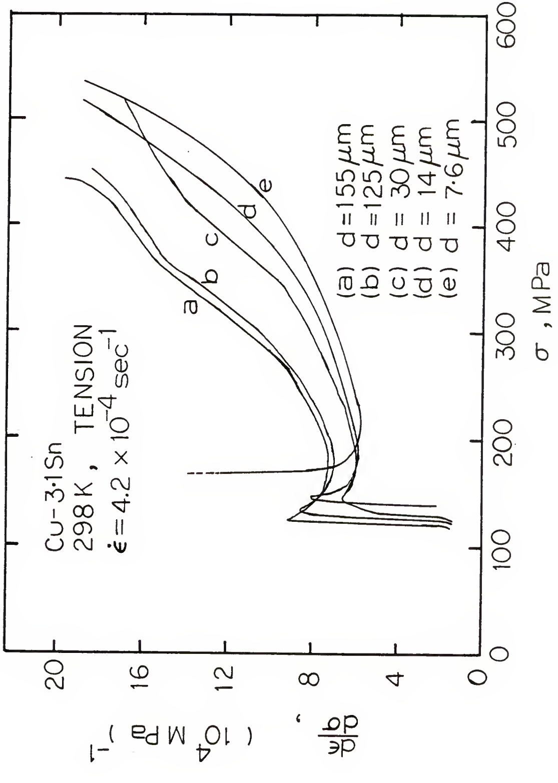
Cu-3·1Sn
298 K , TENSION
ε̇ = 4.2 × 10⁻⁴ sec⁻¹
a
b
c
d
e
(a) d = 155 μm
(b) d = 125 μm
(c) d = 30 μm
(d) d = 14 μm
(e) d = 7·6 μm
σ , MPa
0
100
200
300
400
500
600
dσ/dε , (10⁴ MPa)⁻¹
0
4
8
12
16
20

Figure 54

The variation of $d\varepsilon/d\sigma$ with σ for Cu-4.9 at. pct. Sn tensile specimens having various mean grain intercepts at 77K.

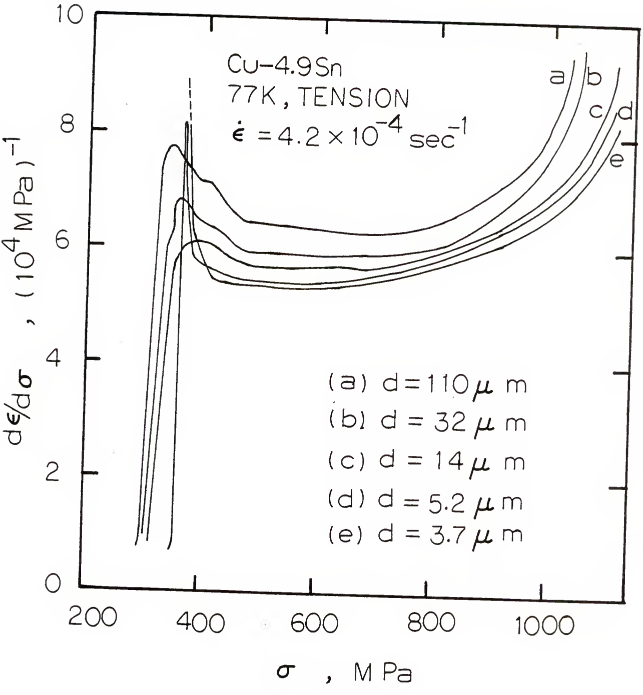
Cu–4.9Sn
77K, TENSION
$\dot{\epsilon} = 4.2 \times 10^{-4}\ \mathrm{sec}^{-1}$
a
b
c
d
e
(a) d = 110 μ m
(b) d = 32 μ m
(c) d = 14 μ m
(d) d = 5.2 μ m
(e) d = 3.7 μ m
$d\epsilon/d\sigma$, $(10^4\ \mathrm{MPa})^{-1}$
0
2
4
6
8
10
200
400
600
800
1000
σ , M Pa

Figure 55

The variation of $d\varepsilon/d\sigma$ with σ for Cu-3.1 at. pct. Sn tensile specimens having various mean grain intercepts at 77K. The circles represent the start of twinning. The triangles represent twin intersections within many grains.

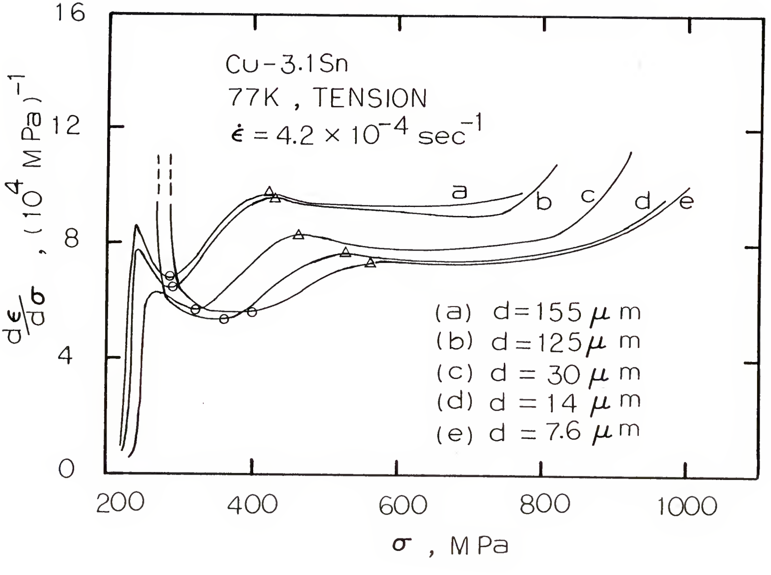
Cu-3.1Sn
77K , TENSION
$\dot{\epsilon} = 4.2 \times 10^{-4}\ \mathrm{sec}^{-1}$
a
b
c
d
e
(a) d=155 μm
(b) d=125 μm
(c) d = 30 μm
(d) d = 14 μm
(e) d = 7.6 μm
$\frac{d\epsilon}{d\sigma}$, $(10^4\ \mathrm{MPa})^{-1}$
0
4
8
12
16
200
400
600
800
1000
σ , MPa

$d\varepsilon/d\sigma$ before the familiar stages are observed. This difference is due to the existence of yield points in the stress-strain curves of specimens having fine grains. Consider the curves "d" and "e" for specimens with mean intercepts of 5.2 and 3.7 μm, respectively. At a true stress of about 350 MPa, the 3.7 μm specimen has a higher work-hardening rate (or lower $d\varepsilon/d\sigma$) than the 5.2 μm specimen. However, the curves "d" and "e" cross each other after twin intersections have occurred in the 5.2 μm specimen at $\sigma \simeq 450$ MPa. Beyond this point, the 5.2 μm specimen has a higher work-hardening rate than the specimen with a mean intercept of 3.7 μm.

Variation of $d\varepsilon/d\sigma$ with σ for Cu-3.1 at. pct. Sn at 298K is indicated in Figure 53 for mean intercepts ranging from 7.6 to 155 μm. The curve "e" shows the presence of a yield point in the stress-strain data. The curves "d" and "e" do not show the typical inflections observed in the other cases. This may be due to a very low degree of twinning in these two fine-grained specimens. Also, notice that the curve "c" crosses "d" when $\sigma \simeq 480$ MPa. After this, the work-hardening rate is higher in the 30 μm material.

The crossing of $d\varepsilon/d\sigma$ versus σ curves and the resulting higher work-hardening rates of specimens having coarser grain sizes may be due to the larger amount of twinning deformation in the coarse-grained material.

The $d\varepsilon/d\sigma$ versus σ variation at 77K for Cu-4.9 at. pct. Sn has been discussed earlier. This behavior appears to be independent of grain size (Figure 54). The upward inflections are absent in all these curves implying the formation of twins on intersecting planes at the nucleation stage itself.

Figure 55 shows the $d\varepsilon/d\sigma$ versus σ curves for Cu-3.1 at. pct. Sn tensile specimens deformed at 77K. Five curves are plotted here for mean intercepts ranging from 7.6 to 155 μm. Note that the inflections are well defined in these low temperature curves. The fine grain size specimens have yield points as seen in curves "d" and "e." All the curves have upward inflections at the start of twinning. Also, constant work-hardening regions are observed after twin intersections have occurred in many grains.

Based on the above observations, it can be concluded that the work-hardening rate is largely determined by the initial boundary area. The work-hardening rate increases as the boundary area is increased. However, in some cases, coarse-grained specimens tend to have a higher work-hardening rate. This is due to the higher degree of twinning in the coarse-grained specimens. It appears that the general effect of mechanical twinning is to change the rate at which the work-hardening rate decreases along a stress-strain curve.

Vöhringer[28] has studied the role of mean grain intercept in determining the twinning stress. For the room temperature deformation of Cu-4.9 at. pct. Sn he has reported a linear relation between σ_t and $d^{-1/2}$, where σ_t is the twinning stress and d is the mean grain intercept. In the case of Cu-15 at. pct. Zn he found a linear relation between σ_t and d^{-1} rather than $d^{-1/2}$. Vöhringer used a limited range of mean grain intercepts compared to the present work. In the present set of data, a plot of σ_t versus $d^{-1/2}$ does not show a linear relation between these two variables. However, a linear variation was found between σ_t and S_V, where S_V represents the sum of the areas of grain boundaries and annealing twin boundaries in the material. The values of S_V were obtained by the relation

$$S_V = \frac{2}{d}$$

where d is the mean intercept.

The variation of σ_t with S_V for the room temperature deformation of Cu-4.9 at. pct. Sn is shown in Figure 56. A similar plot for the deformation of Cu-3.1 at. pct. Sn at 77K is shown in Figure 57. A linear dependence of σ_t on S_V is evident in both these figures. The variation of another parameter, σ_i, is also indicated in these plots. The term σ_i is defined as the stress at which $d\varepsilon/d\sigma$ values tend to level off in the $d\varepsilon/d\sigma$ versus σ plots. The data show that σ_i also varies linearly with S_V. Further, it is observed that both σ_t and σ_i have a similar dependence on S_V. The general implication from these results is that the twinning stress is increased as the boundary area is increased. The stress for twinning on intersecting planes is also affected in a similar manner. The critical strain for the start of

Figure 56

The variation of σ_t and σ_i with S_V for Cu-4.9 at. pct. Sn tensile specimens at 298K.

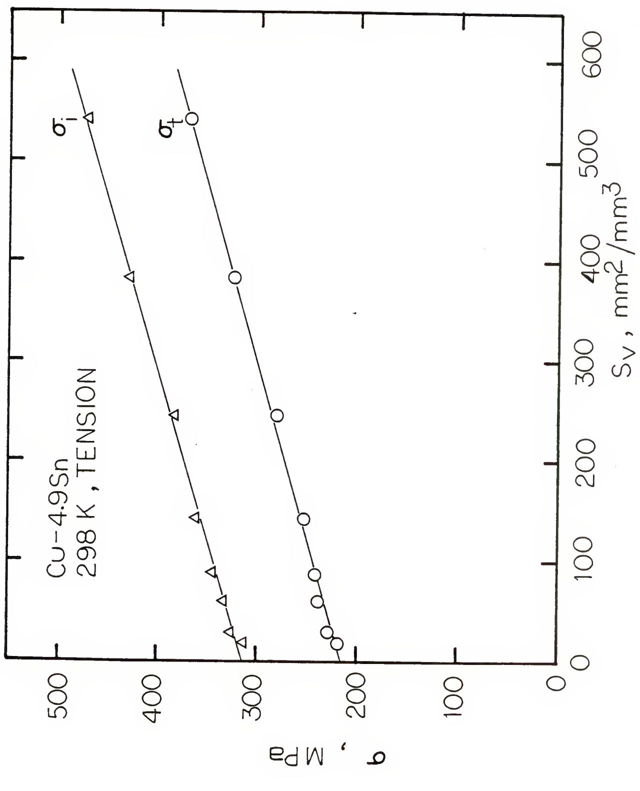
Cu-4.9Sn
298 K , TENSION
σ_i
σ_t
σ , MPa
0
100
200
300
400
500
S_V , mm^2/mm^3
0
100
200
300
400
500
600

Figure 57

The variation of σ_t and σ_i with S_V for Cu-3.1 at. pct. Sn tensile specimens at 77K.

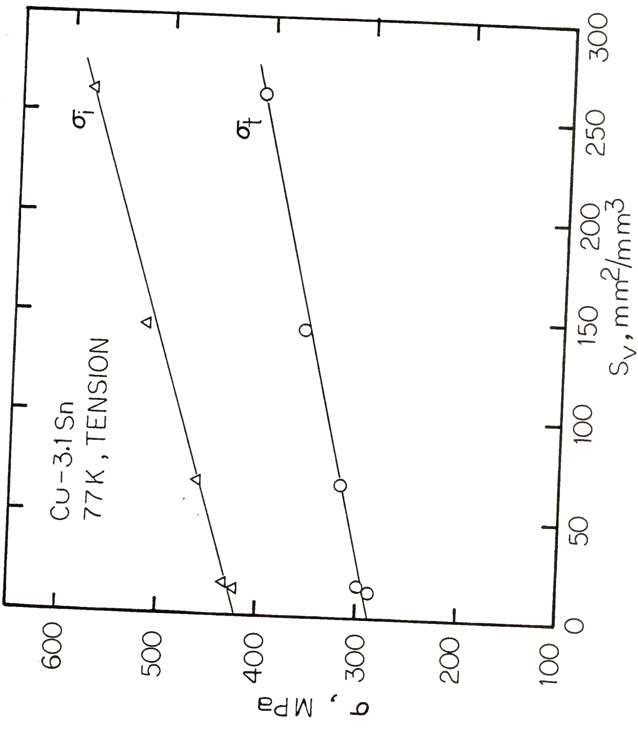
Cu-3.1 Sn
77 K, TENSION
σ_i
σ_f
σ, MPa
100
200
300
400
500
600
0
50
100
150
200
250
300
S_V, mm^2/mm^3

twinning, ε_c, is found to increase linearly with increasing S_V as shown in Figures 58 and 59. The strain corresponding to twin intersections, ε_i, also has a similar dependence on S_V as indicated in these plots. These factors are important in determining the extent of twinning in the specimens.

The dependence of twinning stress on the mean grain intercept has been explained by Vöhringer[28] in terms of a dislocation model. He assumed the presence of a stress concentration due to a pile-up of dislocations at twin nucleation sites. Further, he suggested that this stress concentration increases with mean intercept. This stress concentration is assumed to aid the nucleation of twins. Consequently, a coarse-grained sample can twin at a lower stress than a fine-grained material. However, direct experimental support for this pile-up model is lacking.

5.7 The Dependence of Flow Stress on Boundary Area

In general, the strength of metals increases with a decrease in the mean grain intercept. This effect has been reported in a number of cases to follow the Hall-Petch relation[45,46] .

$$\sigma = \sigma_i + k\, d^{-1/2}$$

where σ is the tensile yield or flow stress, d is the mean intercept, and σ_i and k are material constants. However, several exceptions to this empirical equation have also been

Figure 58

The variation of ε_c and ε_i with S_V for Cu-4.9 at. pct. Sn tensile specimens at 298K.

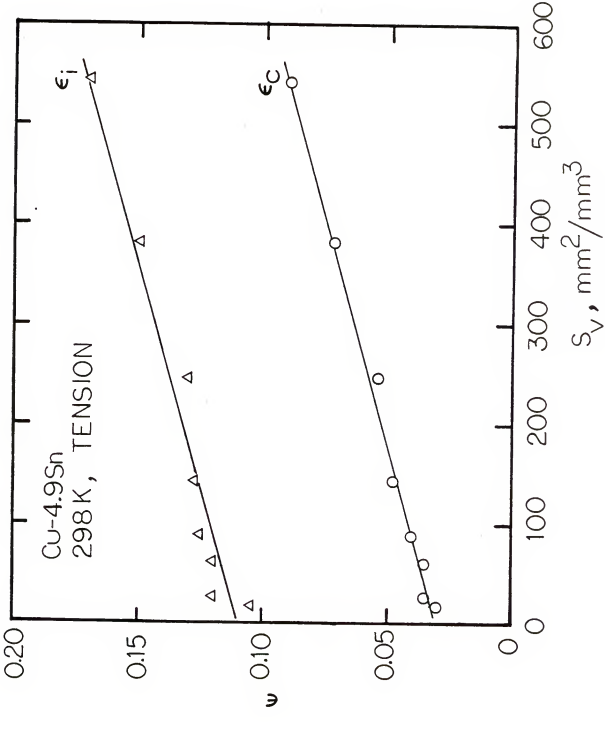
Cu-4.9Sn
298K, TENSION
ϵ_i
ϵ_c
ϵ
0.20
0.15
0.10
0.05
0
0
100
200
300
400
500
600
S_v, mm^2/mm^3

Figure 59

The variation of ε_c and ε_i with S_V for Cu-3.1 at. pct. Sn tensile specimens at 77K.

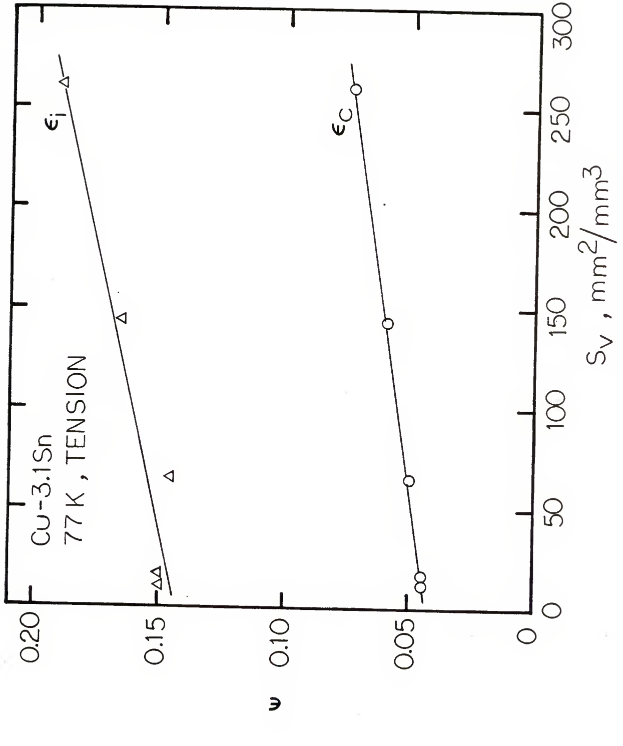
Cu-3.1Sn
77 K , TENSION
ϵ_i
ϵ_c
ϵ
0.20
0.15
0.10
0.05
0
0
50
100
150
200
250
300
S_V , mm^2/mm^3

reported in the literature. Thus a linear dependence of hardness on the total boundary area, S_V, has been found in recrystallized copper-zinc alloys.[47] The deviations from the Hall-Petch relation have been explained in terms of specimen size effects,[48,49] dislocation cell size,[50,51] etc. The flow stress values obtained in this work for copper-tin alloy specimens having various mean intercepts do not obey the Hall-Petch equation. The σ vs. S_V plots were also nonlinear. Figures 60 to 63 show the σ vs. S_V plots for Cu-4.9 at. pct. Sn and Cu-3.1 at. pct. Sn tensile specimens deformed at 298 and 77K. The variation of σ_t and σ_i with S_V is also indicated by dashed lines in Figures 60 and 63. The flow stress varies linearly with S_V only at small strains. The plots tend to be nonlinear at large strains. It is significant that the nonlinearity in these plots begins to appear after the formation of mechanical twins in the structure. The flow stresses in coarse-grained specimens are lower than expected. This should be related to the bigger drop in work-hardening rate that occurs due to the greater degree of twinning in coarse-grained material.

5.8 The Dependence of Flow Stress on the Intertwin Spacing

Rémy[31] assumed that twinning decreases the mean intercept and that once twinning is well underway, the flow stress varies as Δ^{-1} where Δ is the mean free path between twins. However, the data obtained in the present work clearly demonstrate that Rémy's model concerning the effect

Figure 60

The variation of σ with S_V for Cu-4.9 at. pct. Sn tensile specimens deformed to various strains at 298K. The dashed lines indicate σ_t and σ_i.

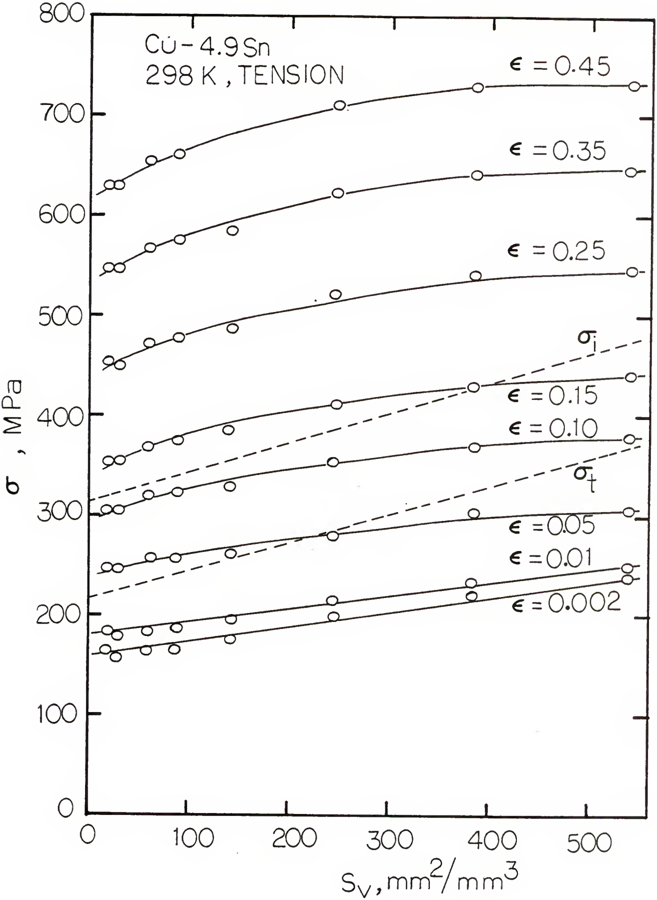
Cu-4.9Sn
298 K, TENSION
ε = 0.45
ε = 0.35
ε = 0.25
σ_i
ε = 0.15
ε = 0.10
σ_t
ε = 0.05
ε = 0.01
ε = 0.002
σ, MPa
800
700
600
500
400
300
200
100
0
0
100
200
300
400
500
S_V, mm^2/mm^3

Figure 61

The variation of σ with S_V for Cu-3.1 at. pct. Sn tensile specimens deformed to various strains at 298K.

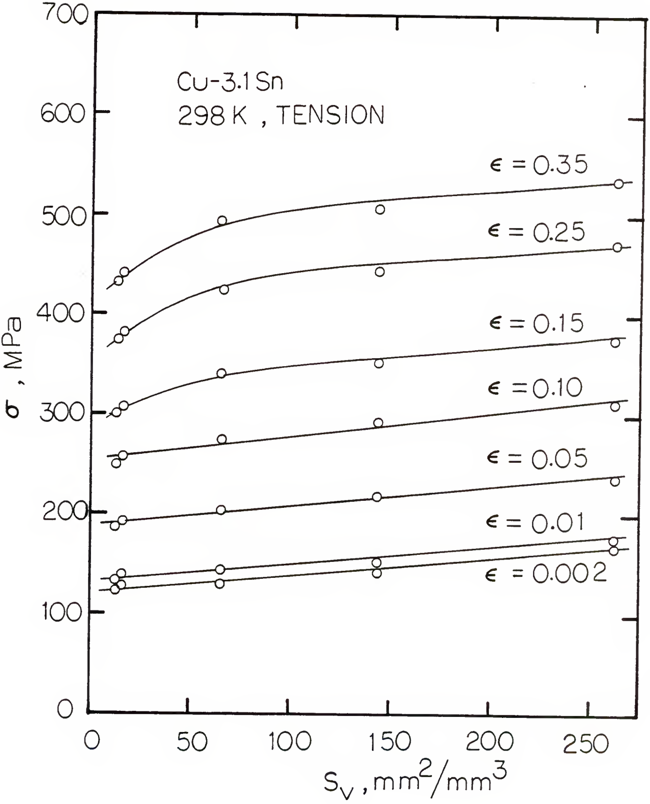
Cu-3.1 Sn
298 K , TENSION
$\epsilon = 0.35$
$\epsilon = 0.25$
$\epsilon = 0.15$
$\epsilon = 0.10$
$\epsilon = 0.05$
$\epsilon = 0.01$
$\epsilon = 0.002$
σ , MPa
0
100
200
300
400
500
600
700
0
50
100
150
200
250
S_V , mm^2/mm^3

Figure 62

The variation of σ with S_V for Cu-4.9 at. pct. Sn tensile specimens deformed to various strains at 77K.

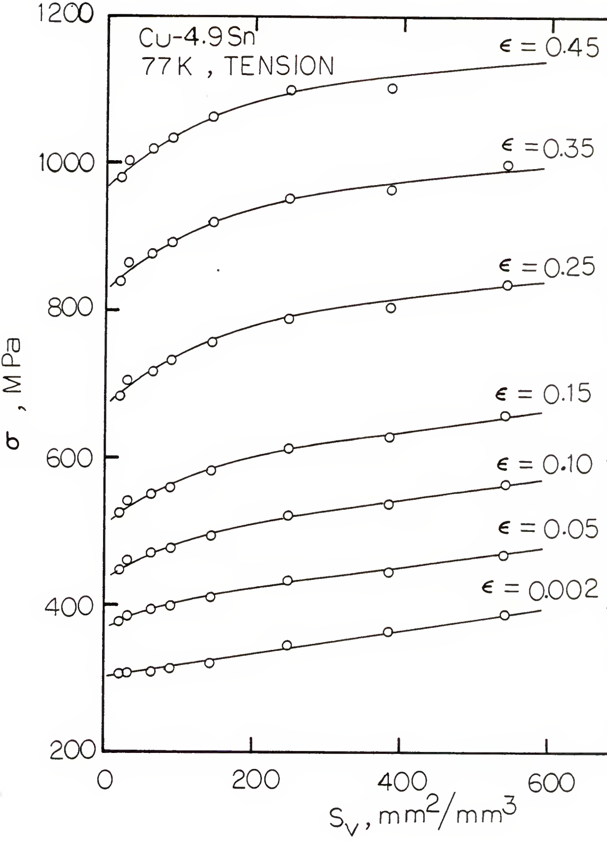
Cu-4.9 Sn
77 K , TENSION
ϵ = 0.45
ϵ = 0.35
ϵ = 0.25
ϵ = 0.15
ϵ = 0.10
ϵ = 0.05
ϵ = 0.002
1200
1000
800
600
400
200
σ , MPa
0
200
400
600
Sv , mm2/mm3

Figure 63

The variation of σ with S_V for Cu-3.1 at. pct. Sn tensile specimens deformed to various strains at 77K. The dashed lines indicate σ_t and σ_i.

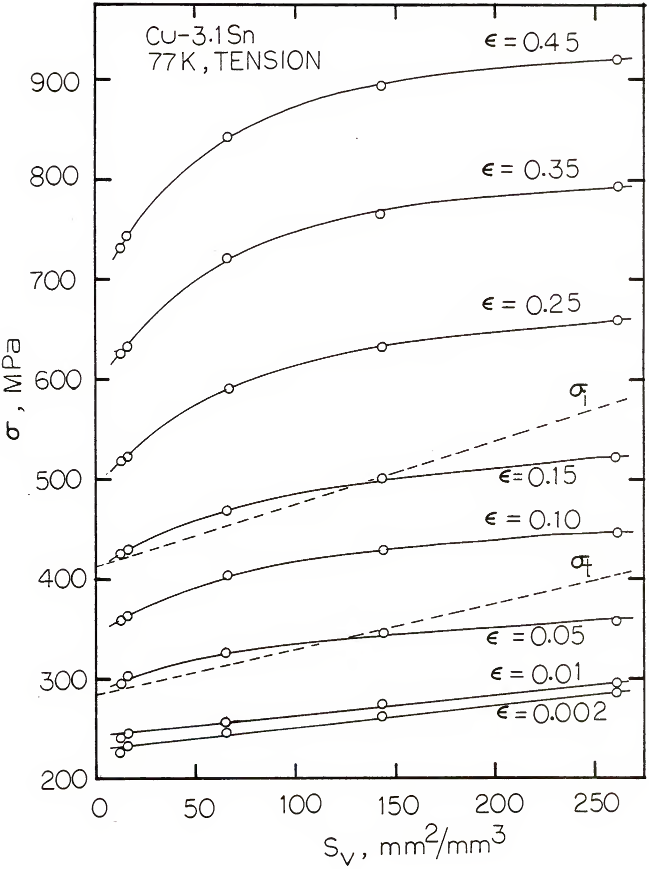
Cu-3.1Sn
77K, TENSION
ε = 0.45
ε = 0.35
ε = 0.25
σi
ε=0.15
ε = 0.10
σf
ε = 0.05
ε = 0.01
ε = 0.002
σ, MPa
900
800
700
600
500
400
300
200
0
50
100
150
200
250
Sv, mm2/mm3

of twinning on the stress-strain curve of a polycrystalline material needs to be modified. He assumes that the twins are uniformly distributed throughout the matrix. But as the present results have shown, only a fraction of the structure twins due to the inherent <111>-<100> duplex texture. This means that a simple parameter such as Δ is not sufficient to account for the effect of heterogeneous twinning. The results obtained in the present study imply that one should more properly treat the structure in terms of a component that does not twin and one that does twin in which the mean free path for dislocations is decreased by twinning. Further, Rémy[31] assumed that there is no deformation within mechanical twins. This assumption is not in agreement with the slip line arrangement shown in Figure 64. This figure shows two mechanical twin bands within an annealing twin. Close inspection of the mechanical twin bands reveals slip lines crossing them.

5.9 Suggestions for Future Work

The work-hardening rate is reduced after the nucleation of mechanical twins. However, when twins intersect within many grains, an increase in the work-hardening rate is observed. These two aspects should be considered while developing relations between the flow stress and microstructural parameters. The structure-property relationships should also treat the inherent <111>-<100> duplex texture which leads to heterogeneous twinning.

Figure 64

Photomicrograph showing the surface of a Cu-4.9 at. pct. Sn tensile specimen (d = 32 μm) which was prestrained (ε = 0.06), etched to show mechanical twins and restrained (ε = 0.015) at 298K. Mechanical twin bands are observed within an annealing twin. Inspection of the mechanical twin bands shows slip lines crossing them. Magnification 600 times.

Another interesting observation is that the volume fraction of twins in Cu-3.1 at. pct. Sn decreases rapidly in the temperature interval from 500 to 600K. It is worth exploring if this drop is due to a recovery process.

CHAPTER 6
CONCLUSIONS

From the data obtained in this investigation the following conclusions can be reached within the limits of experimentation:

1. The nucleation of mechanical twins occurs predominantly at grain boundaries, grain edges and annealing twin boundaries.
2. With the aid of twin trace measurements made on transverse sections of deformed specimens it was deduced that the Cu-4.9 at. pct. Sn alloy had a duplex <111>-<100> wire texture with about 65 pct. of the grains in the <111> orientation, 25 pct. in the <100> orientation, and 10 pct. in other general orientations.
3. During tensile deformation of Cu-4.9 at. pct. Sn twinning occurs preferentially in the 65 pct. of the grains with a <111> orientation while in compression twinning occurs in the 25 pct. of the grains with a <100> orientation. These results are in accord with the magnitudes of the respective Schmid factors for twinning in the two types of specimens taking into account the polar nature of the twinning shear.

4. In the true strain range 0-0.20, the volume fraction of twins in Cu-4.9 at. pct. Sn deformed at 298K was observed to be larger in the compression specimens than in the tensile specimens in spite of the fact that the fraction of the structure that twins in compression is much smaller than that which twins in tension. In this regard, it is considered significant that the Schmid factor for twinning in the <100> grains is 1.5 times that in the <111> grains.
5. The true stress-true strain curves in tension and compression differ significantly with the compression curve lying below the tensile curve.
6. Vöhringer's observation that the start of twinning is accompanied by a decrease in the work-hardening rate was confirmed in Cu-4.9 at. pct. Sn, Cu-3.1 at. pct. Sn and Co-40 at. pct. Ni alloys. This effect can be used to rationalize the difference between the tensile and compressive stress-strain curves.
7. In the case of room temperature deformation, at low strains twins tend to be parallel and form largely on one crystallographic plane in any given region of the structure. This suggests that initially twinning should not strongly influence the flow stress level. However, at larger strains, the tendency for twins to form on intersecting planes

should act to increase the flow stress due to the subdivision of structure.

8. Microhardness tests made in twinned and untwinned regions of Cu-4.9 at. pct. Sn compression specimens prestrained to various amounts at 298K show that at large strains twinning increases the hardness or strength.
9. At 77K, twin nucleation in Cu-4.9 at. pct. Sn occurs on intersecting planes. The volume fraction of twins increases as the test temperature is lowered. These factors lead to high work-hardening rate and uniform strain at low temperatures.
10. The twinning stress σ_t increases linearly with increasing S_V, the total boundary area in the starting material. A similar relation is observed between σ_i, the stress corresponding to twin intersections within many grains, and S_V. Thus, the twinned volume fraction is higher in the coarse-grained specimens than in the fine-grained ones.
11. The stress-strain curves are largely determined by the initial boundary area. The curves shift to higher flow stress values as the mean grain intercept is reduced. The main role of twinning appears to be to change the way in which the work-hardening rate varies along a stress-strain curve. Within certain mean intercept and strain intervals, the work-hardening rate increases as the mean intercept

is increased. This effect is due to the higher degree of twinning in coarse-grained material.

REFERENCES

1. V. F. Zackay, E. R. Parker, D. Fahr, and R. Busch: Trans. ASM, 1967, vol. 60, pp. 252-259.

2. D. Bhandarkar, V. F. Zackay, and E. R. Parker: Met. Trans., 1972, vol. 3, pp. 2619-2631.

3. A. M. Garde and R. E. Reed-Hill: Met. Trans., 1971, vol. 2, pp. 2885-2888.

4. E. A. Loria, G. H. Keith, and E. A. Rowe: Bureau of Mines Report of Investigations 6716, U.S. Dept. of the Interior, 1965.

5. C. N. Reid, A. Gilbert, and G. T. Hahn: Acta Met., 1966, vol. 14, pp. 975-983.

6. R. P. Carreker, Jr.: Trans. TMS-AIME, 1957, vol. 209, pp. 112-115.

7. W. N. Roberts: Trans. TMS-AIME, 1964, vol. 230, pp. 372-377.

8. Z. Nishiyama, M. Oka, and H. Nakagawa: Trans. Jpn. Inst. Met., 1965, vol. 6, pp. 88-92.

9. K. S. Raghavan, A. S. Sastri, and M. J. Marcinkowski: Trans. TMS-AIME, 1969, vol. 245, pp. 1569-1575.

10. A. J. Baker and B. F. Peters: Trans. Jpn. Inst. Met., 1968, vol. 9, pp. 919-925.

11. A. H. Cottrell and B. A. Bilby: Phil. Mag., 1951, vol. 42, pp. 573-581.

12. T. H. Blewitt, R. R. Cotlman, and J. K. Redman: J. Appl. Phys., 1957, vol. 28, pp. 651-660.

13. P. Haasen: Phil. Mag., 1958, vol. 3, pp. 384-418.

14. H. Suzuki and C. S. Barrett: Acta Met., 1958, vol. 6, pp. 156-165.

15. B. Ramaswami: J. Appl. Phys., 1965, vol. 36, pp. 2569-2570.

16. P. Haasen and A. King: Z. Metallk., 1960, vol. 51, pp. 722-736.

17. E. Peissker: Z. Metallk., 1965, vol. 56, pp. 155-164.

18. P. R. Thornton and T. E. Mitchell: Phil. Mag., 1962, vol. 7, pp. 361-375.

19. J. A. Venebles: J. Phys. Chem. Solids, 1964, vol. 25, pp. 685-692.

20. G. Y. Chin, W. F. Hosford, and D. R. Mendorf: Proc. Roy. Soc., 1959, vol. A309, pp. 433-456.

21. N. Narita and J. Takamura: Phil. Mag., 1974, vol. 29, pp. 1001-1028.

22. B. A. Bilby and A. G. Crocker: Proc. Roy. Soc., 1965, vol. A288, pp. 240-255.

23. N. Thompson: Phys. Soc. Proc., 1953, vol. B66, pp. 481-492.

24. J. A. Venebles: Phil. Mag., 1961, vol. 6, pp. 379-396.

25. S. Miura, J. Takamura, and N. Narita: Trans. Jpn. Inst. Met., 1968, vol. 9, pp. 555-562.

26. S. Mahajan and G. Y. Chin: Acta Met., 1973, vol. 21, pp. 1353-1363.

27. O. Vöhringer, Mater. Sci. Eng., 1968/69, vol. 3, pp. 299-302.

28. O. Vöhringer: Second Int. Conf. on Strength of Metals and Alloys, pp. 294-298, ASM, Metals Park, Ohio, 1970.

29. O. Vöhringer: Z. Metallk., 1976, vol. 67, pp. 518-524.

30. O. Vöhringer: Metallurgie, 1976, vol. 30, pp. 1150-1160.

31. L. Rémy: Acta Met., 1978, vol. 26, pp. 443-451.

32. M. Cook and E. C. Larke: J. Inst. Metals, 1945, vol. 71, pp. 371-390.

33. R. E. Reed-Hill, C. R. Smeal, and L. Lee: Trans. TMS-AIME, 1964, vol. 230, pp. 1019-1024.

34. R. T. DeHoff and F. N. Rhines: Quantitative Microscopy, pp. 29-32, McGraw-Hill Book Company, New York, 1968.

35. M. P. Drazin and H. M. Otte: Table for Determining Cubic Crystal Orientation, Harrod Company, Baltimore, Maryland, 1964.

36. C. S. Barrett and T. B. Massalski: Structure of Metals, 3rd Edition, p. 569, McGraw-Hill Book Company, New York, 1966.

37. E. Schmid and W. Boas: Kristallplastizät, Julius Springer, Berlin, 1935.

38. J. A. Venebles: AIME Conf. Deformation Twinning, p. 77, Gordon and Breach Science Publishers, Inc., New York, 1964.

39. H. Fujita and T. Mori: Scr. Met., 1975, vol. 9, pp. 631-636.

40. T. Mori and H. Fujita: Trans. Jpn. Inst. Met., 1977, vol. 18, pp. 17-24.

41. E. H. Köster, A. R. Thölen, and A. Howie: Phil. Mag., 1964, vol. 10, pp. 1093-1095.

42. D. Tabor: Proc. Roy. Soc., 194, vol. A192, pp. 247-274.

43. J. Nunes and F. R. Larson: J. Inst. Metals, 1962/63, vol. 91, pp. 114-117.

44. M. Blicharski and S. Gorczyca: Metl. Sci., 1978, vol. 12, pp. 303-312.

45. E. O. Hall: Proc. Phys. Soc., 1951, vol. B64, pp. 747-753.

46. N. J. Petch: J. Iron and Steel Inst., 1953, vol. 174, pp. 25-28.

47. J. E. Lemons: Ph.D. Dissertation, University of Florida, Gainesville (1968).

48. S. Miyazaki and H. Fujita: Trans. Jpn. Inst. Met., 1978, vol. 19, pp. 438-444.

49. S. Miyazaki, K. Shibata, and H. Fujita: Acta Met., 1979, vol. 27, pp. 855-862.

50. H. Fujita and T. Tabata: Acta Met., 1973, vol. 21, pp. 355-365.

51. T. Tabata, K. Takagi, and H. Fujita: Trans. Jpn. Inst. Met., 1975, vol. 16, pp. 569-579.

BIOGRAPHICAL SKETCH

Setumadhavan Krishnamurthy was born on February 27, 1952, in Nanjangud, Karnataka State, India. He attended local schools and entered the Indian Institute of Technology at Bombay in July 1969. In April 1974 he received a degree of Bachelor of Technology in metallurgical engineering from that institution. He entered graduate school in September 1974 at Washington State University and received a Master of Science degree in materials science in June 1976. He later attended the University of Florida to continue graduate work towards a degree of Doctor of Philosophy in materials science and engineering.

He is a member of Alpha Sigma Mu, Tau Beta Pi and the Metallurgical Society of AIME.

He is married to the former Girija Srikantia from Mysore.

I certify that I have read this study and that in my opinion it conforms to acceptable standards of scholarly presentation and is fully adequate, in scope and quality, as a dissertation for the degree of Doctor of Philosophy.

R. E. Reed-Hill, Chairman
Professor of Materials Science
and Engineering

I certify that I have read this study and that in my opinion it conforms to acceptable standards of scholarly presentation and is fully adequate, in scope and quality, as a dissertation for the degree of Doctor of Philosophy.

E. D. Verink, Jr.
Professor of Materials Science
and Engineering

I certify that I have read this study and that in my opinion it conforms to acceptable standards of scholarly presentation and is fully adequate, in scope and quality, as a dissertation for the degree of Doctor of Philosophy.

R. T. DeHoff

R. T. DeHoff
Professor of Materials Science
and Engineering

I certify that I have read this study and that in my opinion it conforms to acceptable standards of scholarly presentation and is fully adequate, in scope and quality, as a dissertation for the degree of Doctor of Philosophy.

E. Dow Whitney

E. D. Whitney
Professor of Materials Science
and Engineering

I certify that I have read this study and that in my opinion it conforms to acceptable standards of scholarly presentation and is fully adequate, in scope and quality, as a dissertation for the degree of Doctor of Philosophy.

M. A. Eisenberg
Professor of Engineering
Sciences

This dissertation was submitted to the Graduate Faculty of the College of Engineering and to the Graduate Council, and was accepted as partial fulfillment of the requirements for the degree of Doctor of Philosophy.

December 1981

Wayne H. Chen
Dean, College of Engineering

Dean for Graduate Studies and
Research